AUTOREGRESSIVE MOVING-AVERAGE ATTENTION MECHANISM FOR TIME SERIES FORECASTING

Jiecheng Lu[1], **Xu Han**[2], **Yan Sun**[1], **Shihao Yang**[1]
[1]Georgia Institute of Technology [2]Amazon Web Services
{jlu414,yansun}@gatech.edu, icyxu@amazon.com
shihao.yang@isye.gatech.edu

ABSTRACT

We propose an Autoregressive (AR) Moving-average (MA) attention structure that can adapt to various linear attention mechanisms, enhancing their ability to capture long-range and local temporal patterns in time series. In this paper, we first demonstrate that, for the time series forecasting (TSF) task, the previously overlooked decoder-only autoregressive Transformer model can achieve results comparable to the best baselines when appropriate tokenization and training methods are applied. Moreover, inspired by the ARMA model from statistics and recent advances in linear attention, we introduce the full ARMA structure into existing autoregressive attention mechanisms. By using an indirect MA weight generation method, we incorporate the MA term while maintaining the time complexity and parameter size of the underlying efficient attention models. We further explore how indirect parameter generation can produce implicit MA weights that align with the modeling requirements for local temporal impacts. Experimental results show that incorporating the ARMA structure consistently improves the performance of various AR attentions on TSF tasks, achieving state-of-the-art results. The code implementation is available at the following link.

1 INTRODUCTION

In recent years, autoregressive (AR) decoder-only Transformer-based models (Vaswani, 2017; Radford, 2018) have been widely used in sequence modeling tasks across fields such as NLP (Brown et al., 2020; Touvron et al., 2023), CV (Chen et al., 2020; Esser et al., 2021; Chang et al., 2022), and audio (Borsos et al., 2023). This structure is well-suited for various sequential generation and prediction tasks. However, in typical sequence modeling tasks like time series forecasting (TSF), there has been less exploration of this architecture compared to other structures. Most of the best-performing recent TSF models are encoder-only Transformers (Liu et al., 2024a; Nie et al., 2022), MLPs (Das et al., 2023; Lu et al., 2024), or even linear models (Zeng et al., 2023; Xu et al., 2024). The few relevant discussions mainly focus on using pretrained autoregressive LLMs or similar structures for few-shot and zero-shot prediction (Gruver et al., 2023; Jin et al., 2024; Das et al., 2024; Liu et al., 2024b), with little research directly evaluating their TSF performance in end-to-end training. Therefore, this paper will first briefly demonstrate that with appropriate tokenization and training methods, a basic AR Transformer is enough to achieve results comparable to the state-of-the-art (SOTA) baselines, as shown in Fig. 1 and Fig. 2.

Recently, efficient linear AR attention variants have been explored and developed (Katharopoulos et al., 2020; Hua et al., 2022), reducing the time complexity of standard softmax attention from $O(N^2)$ to $O(N)$. Researchers have found that adding a gating decay factor or a similar exponential moving average (EMA) structure to AR structure, as in gated linear attention (Ma et al., 2022; Yang et al., 2024), enhances linear attention's ability to model local patterns and improves performance. The success of these approaches inspired us to introduce a more comprehensive full autoregressive moving-average (ARMA) structure into existing AR attention mechanisms and explore the performance of the ARMA Transformers in TSF.

In TSF models, EMA, connecting back to the historic work of Holt-Winters (Winters, 1960; Holt, 2004), focuses on smoothed local data, which improves the modeling of short-term fluctuations but

reduces the ability to capture long-term information. In contrast, ARMA, connecting back to the historic work of Box-Jenkins (Box et al., 1974), a classic structure in TSF, considers both historical data and the cumulative impact of prediction errors. This allows it to handle and decouple long-term and short-term effects, significantly improving forecasting performance on data with complicated temporal patterns.

We propose the ARMA attention mechanism, which integrates a moving-average (MA) term into various existing AR attention mechanisms. Our method improves the TSF performance of AR Transformers without significantly increasing computational costs, maintaining $O(N)$ time complexity and original parameter size. We design an indirect MA weight generation to obtain the MA output without explicitly computing the MA attention matrix, preserving efficiency of linear attentions. We explore specific techniques for generating implicit MA weights to ensure proper decoupling and handling of short-term effects. Extensive experiments and visualization analyses demonstrate that ARMA balances long- and short-term dependencies, significantly improving AR Transformers and achieving state-of-the-art TSF results.

The main contributions of this paper can be summarized as follows:

a) We demonstrate that, with appropriate tokenization and preprocessing methods, an AR Transformer is enough to achieve the level of existing SOTA baselines. Furthermore, the introduction of ARMA attention enables the decoder-only Transformer to outperform SOTA baselines.

b) We propose the ARMA attention mechanism, which introduces an MA term into existing AR attention without increasing time complexity or parameter size. By adding the MA term to various AR attention mechanisms, the resulting ARMA Transformers significantly improve forecasting performance compared to their AR counterparts.

c) We design an indirect MA weight generation method that is computationally efficient while ensuring that the implicit MA weights effectively capture the important short-term effects in TSF, allowing the AR term to focus more on long-term and cyclic patterns.

2 METHOD

2.1 TIME SERIES FORECASTING

In Time Series Forecasting (TSF), the goal is to predict the future part in a multivariate time series $\mathbf{S} \in \mathbb{R}^{L \times C}$, where L is the length of the series, and C is the number of channels or input series. The time series is divided into historical input $\mathbf{S}_I \in \mathbb{R}^{L_I \times C}$, and future data $\mathbf{S}_P \in \mathbb{R}^{L_P \times C}$, where $L = L_I + L_P$, and L_I and L_P represent the lengths of the input and forecasting periods, respectively. The objective is to learn a mapping function $f : \mathbb{R}^{L_I \times C} \to \mathbb{R}^{L_P \times C}$ that predicts the future values $\widehat{\mathbf{S}}_P = f(\mathbf{S}_I)$, given the historical input $\mathbf{S}_I$.

2.2 APPROPRIATE TOKENIZATION FOR AUTOREGRESSIVE FORECASTING

Recently, most time series forecasting research utilizes encoder-decoder or encoder-only Transformers for TSF (Li et al., 2019b; Zhou et al., 2021; Wu et al., 2021; Nie et al., 2022; Liu et al., 2024a), with limited focus on end-to-end decoder-only autoregressive Transformer because of error accumulation issue. For long-term forecasts, The autoregressive Transformers requires iteratively doing one-step prediction, leading to error accumulation and higher MSE compared to non-autoregressive models that generate the entire forecast at once.

To prevent error accumulation, we use an autoregressive Transformer (Fig. 1) that treats one-step prediction as the complete forecast. Inspired by PatchTST (Nie et al., 2022), we adopt a channel-independent approach, predicting each series separately and applying RevIN (Kim et al., 2022) to each. For an input series of length L_I in $\mathbf{S}_I$, we apply non-overlapping patches with a patch size L_P, dividing the input into $N = \frac{L_I+P}{L_P}$ patches, where P is zero-padding for divisibility. This

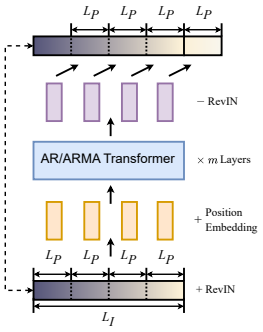

Figure 1: Overall architecture of our decoder Transformer for TSF.

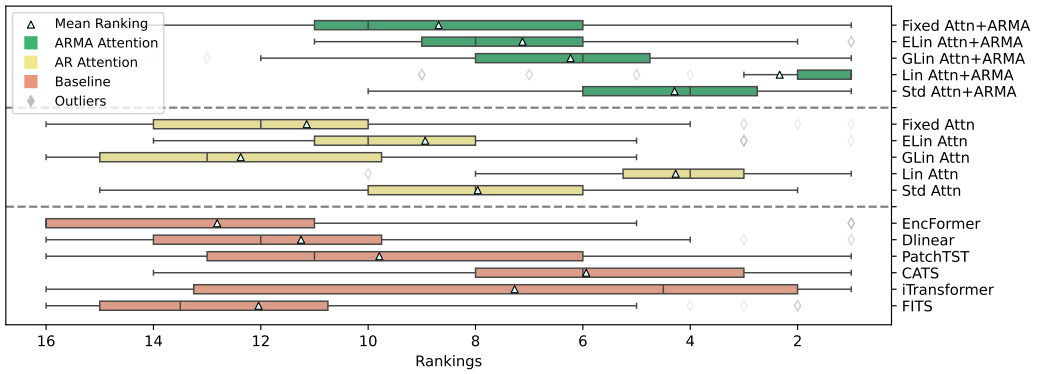

Figure 2: Box plots of performance rankings from 48 sub-experiments across 12 datasets. Green represents ARMA Transformers, yellow AR Transformers, and red the baselines, with triangles indicating mean rankings. AR Transformers perform comparably to baselines, while ARMA Transformers significantly outperform their AR counterparts. See Table 2 and 8 for more details.

ensures that each out-of-sample prediction token covers the entire forecasting length L_P, thereby avoiding error accumulation.

Fig. 2 shows that autoregressive Transformers using this method can achieve performance comparable to existing SOTA models. Additionally, decoder-based architectures may have significant advantages in extended lookback length and varying output horizon, highlighting their potential.

2.3 Preliminaries: decoder-only Transformer

We use a GPT-2–style decoder-only Transformer (Radford et al., 2019) for autoregressive TSF. Token patches of length L_P are linearly projected to d-dimensional vectors and combined with learnable positional embeddings to form the input sequence $\mathbf{X} \in \mathbb{R}^{N\times d}$, where each token is $\boldsymbol{x}_t \in \mathbb{R}^{1\times d}$. Each of the m Transformer layers applies layer normalization $\mathrm{LN}(\cdot)$, attention $\mathrm{Attn}(\cdot)$, and a channel-wise MLP $\mathrm{MLP}(\cdot)$. With single-head softmax attention, a Transformer layer is defined as:

$$\begin{aligned} \mathrm{Attn}(\mathbf{X}) = \mathrm{softmax}\left(\mathbf{M}\odot(\mathbf{Q}\mathbf{K}^\top)\right)\mathbf{V}\mathbf{W}_o, \quad \text{with } \mathbf{Q},\mathbf{K},\mathbf{V} = \mathbf{X}\mathbf{W}_q, \mathbf{X}\mathbf{W}_k, \mathbf{X}\mathbf{W}_v \\ \mathbf{X} := \mathbf{X} + \mathrm{Attn}(\mathrm{LN}(\mathbf{X})), \quad \text{then } \mathbf{X} := \mathbf{X} + \mathrm{MLP}(\mathrm{LN}(\mathbf{X})) \end{aligned} \tag{1}$$

where $\mathbf{W}_q, \mathbf{W}_k, \mathbf{W}_v, \mathbf{W}_o \in \mathbb{R}^{d\times d}$ are the projection matrices for the query, key, value, and output, respectively, and $\mathbf{M} \in \mathbb{R}^{N\times N}$ is the causal mask, defined as $\mathbf{M}_{ij} = 1\{i \geq j\} - \infty \cdot 1\{i < j\}$.

2.4 Preliminaries: efficient linear attention mechanisms

Recent autoregressive efficient attention mechanisms reduce computational complexity from $O(N^2)$ to $O(N)$ by avoiding the explicit calculation of the $N \times N$ attention matrix (Katharopoulos et al., 2020; Choromanski et al., 2021; Hua et al., 2022; Sun et al., 2023). Most of them can be reformulated as parallel linear RNNs with identity or diagonal state updates. Although these efficient attentions do not outperform standard softmax attention for large models, they achieve comparable results on smaller tasks (Katharopoulos et al., 2020; Choromanski et al., 2021). This paper investigates integrating these mechanisms into TSF and shows that adding a moving-average term significantly improves their performance. We begin by expressing the recurrent form of standard softmax attention. For a single head without output projection, let $\boldsymbol{q}_t, \boldsymbol{k}_t, \boldsymbol{v}_t$ be the vectors at step t from $\mathbf{Q}, \mathbf{K}, \mathbf{V}$. The output $\boldsymbol{o}_t$ is given by: $\boldsymbol{o}_t = \frac{\sum_{i=1}^{t} \exp(\boldsymbol{q}_t \boldsymbol{k}_i^\top)\boldsymbol{v}_i}{\sum_{i=1}^{t} \exp(\boldsymbol{q}_t \boldsymbol{k}_i^\top)}$.

Linear attention Linear Attention replaces the $\exp(\boldsymbol{q}_t \boldsymbol{k}_i^\top)$ term in standard attention with a kernel function $k(\boldsymbol{x}, \boldsymbol{y}) = \langle \phi(\boldsymbol{x}), \phi(\boldsymbol{y}) \rangle$, resulting in $\phi(\boldsymbol{q}_t)\phi(\boldsymbol{k}_i)$ (Katharopoulos et al., 2020). This change reduces the time complexity from $O(N^2)$ to $O(N)$ by eliminating the need to compute the full $N \times N$ attention matrix. Instead, it computes $\phi(\boldsymbol{k}_i)^\top \boldsymbol{v}_i$ for each i and aggregates over N. Various kernel functions have been explored, with identity kernels without denominators performing well enough (Mao, 2022; Qin et al., 2022; Sun et al., 2023; Yang et al., 2024). In this setup, Linear

attention can be viewed as an RNN with a hidden state matrix $\boldsymbol{k}_i^\top \boldsymbol{v}_i \in \mathbb{R}^{d\times d}$ that updates using the identity function. The output at each step is: $\boldsymbol{o}_t = \boldsymbol{q}_t \sum_{i=1}^{t} \boldsymbol{k}_i^\top \boldsymbol{v}_i$.

Element-wise linear attention In multi-head linear attention with h heads, we handle h hidden state matrices of size $\frac{d}{h} \times \frac{d}{h}$. When $h = d$, this simplifies to h scalar hidden states, effectively transforming linear attention into a linear RNN with a d-dimensional hidden state vector $\phi(\boldsymbol{k}_i) \odot \boldsymbol{v}_i$ and enabling element-wise computations of $\boldsymbol{q}, \boldsymbol{k}, \boldsymbol{v}$. This approach, also known as the Attention Free Transformer (AFT) (Zhai et al., 2021), is favored for its simplicity and efficiency in recent works (Peng et al., 2023). We adopt the structure in AFT, where $\sigma(\cdot)$ is the sigmoid function, and the output at each step is: $\boldsymbol{o}_t = \sigma(\boldsymbol{q}_t) \odot \frac{\sum_{i=1}^{t} \exp(\boldsymbol{k}_i) \odot \boldsymbol{v}_i}{\sum_{i=1}^{t} \exp(\boldsymbol{k}_i)}$.

Gated linear attention Recent studies have explored adding a forget gate, commonly used in traditional RNNs, to linear attention, allowing autoregressive models to forget past information and focus on local patterns (Mao, 2022; Sun et al., 2023; Qin et al., 2024; Yang et al., 2024). We implement a simple gating mechanism where each input $\boldsymbol{x}_t$ is converted into a scalar between [0, 1] and expanded into a forget matrix $\mathbf{G}_i$ matching the shape of $\boldsymbol{k}_i \boldsymbol{v}_i$. With gating parameters $\mathbf{W}_g \in \mathbb{R}^{d\times 1}$, the output at each step is: $\boldsymbol{o}_t = \boldsymbol{q}_t \sum_{i=1}^{t} \mathbf{G}_i \odot \boldsymbol{k}_i^\top \boldsymbol{v}_i, \;\; \mathbf{G}_i = \prod_{k=1}^{i} \sigma(\boldsymbol{x}_k \mathbf{W}_g) \mathbf{1}^\top \mathbf{1}$.

Fixed Attention We additionally explore an autoregressive structure with fixed, data-independent weights $w_{t,i}$, replacing the dynamically generated attention weights $\phi(\boldsymbol{q}_t)\phi(\boldsymbol{k}_i)$. Without dynamic parameter generation, this becomes a linear layer with a causal mask $\mathbf{M}$ rather than a true attention mechanism. We use this structure to examine the effect of adding a moving-average term. This autoregressive causal linear layer is expressed as: $\boldsymbol{o}_t = \sum_{i=1}^{t} w_{t,i} \boldsymbol{v}_i$.

2.5 ARMA ATTENTION MECHANISM

In these attention mechanisms, the next-step prediction at time t is a weighted sum of all previous values $\boldsymbol{v}_i \in \mathbb{R}^{1\times d}$, with weights $\mathbf{w}_{t,i} \in \mathbb{R}^{1\times d}$ derived from interactions between $\boldsymbol{q}_t$ and $\boldsymbol{k}_i$. Naturally, we can write these attention mechanisms in an AR model structure:

$$\boldsymbol{v}_{t+1} = \boldsymbol{o}_t^{\text{AR}} + \boldsymbol{r}_t = \sum_{i=1}^{t} \mathbf{w}_{t,i} \odot \boldsymbol{v}_i + \boldsymbol{r}_t,$$

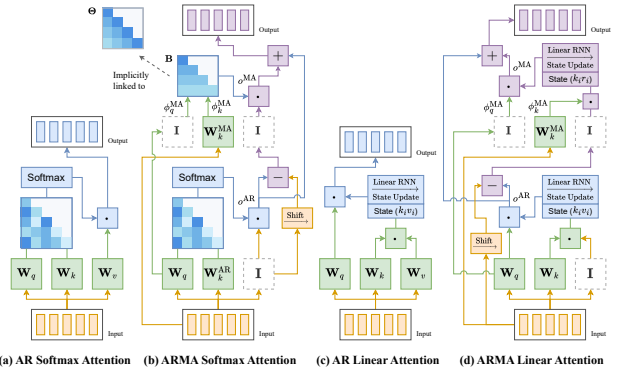

Figure 3: ARMA attention structure with the indirect MA weight generation method applied to softmax and linear attention. See Table 1 for more calculation details.

where $\boldsymbol{r}_t$ is the AR error. In an ARMA model, the MA term captures short-term fluctuations, allowing the AR component to focus on long-term dependencies. Let $\boldsymbol{\epsilon}_t$ be the error after introducing the MA term and $\boldsymbol{\theta}_{t-1,j}$ the MA weights generated by some attention mechanism. We expand the AR error $\boldsymbol{r}_t$ into an MA form and extend the model to an ARMA structure as:

$$\boldsymbol{v}_{t+1} = \boldsymbol{o}_t^{\text{AR}} + \boldsymbol{o}_t^{\text{MA}} + \boldsymbol{\epsilon}_t = \sum_{i=1}^{t} \mathbf{w}_{t,i} \odot \boldsymbol{v}_i + \sum_{j=1}^{t-1} \boldsymbol{\theta}_{t-1,j} \odot \boldsymbol{\epsilon}_j + \boldsymbol{\epsilon}_t, \;\; \boldsymbol{r}_t = \sum_{j=1}^{t-1} \boldsymbol{\theta}_{t-1,j} \odot \boldsymbol{\epsilon}_j + \boldsymbol{\epsilon}_t \quad (2)$$

The structure of the MA output $\boldsymbol{o}_t^{\text{MA}} = \sum_{j=1}^{t-1} \boldsymbol{\theta}_{t-1,j} \odot \boldsymbol{\epsilon}_j$ resembles the AR term and could potentially be computed using an attention mechanism. For simplicity, we consider a single channel of the d-dimensional space, with other channels an be handled in parallel. We express the matrix form

of the $\boldsymbol{r}_t$ in Eq. 2 for one channel as:

$$\begin{pmatrix} r_1 \\ r_2 \\ \vdots \\ r_t \end{pmatrix} = \begin{pmatrix} 0 & 0 & \cdots & 0 & 0 \\ \theta_{1,1} & 0 & \cdots & 0 & 0 \\ \theta_{2,1} & \theta_{2,2} & \cdots & 0 & 0 \\ \vdots & \vdots & \ddots & \vdots & \vdots \\ \theta_{t-1,1} & \theta_{t-1,2} & \cdots & \theta_{t-1,t-1} & 0 \end{pmatrix} \begin{pmatrix} \epsilon_1 \\ \epsilon_2 \\ \vdots \\ \epsilon_t \end{pmatrix} + \begin{pmatrix} \epsilon_1 \\ \epsilon_2 \\ \vdots \\ \epsilon_t \end{pmatrix} \tag{3}$$
$$\mathbf{r} = (\mathbf{I} + \mathbf{\Theta})\epsilon, \;\; \epsilon = (\mathbf{I} + \mathbf{\Theta})^{-1}\mathbf{r},$$

where $\mathbf{\Theta}$ is a strictly lower triangular matrix of MA weights for this channel. Once the attention mechanism determines $\boldsymbol{o}_t^{\text{AR}}$ and $\boldsymbol{\theta}_{t-1,j}$, we can calculate $\boldsymbol{r}_j = \boldsymbol{v}_{j+1} - \boldsymbol{o}_j^{\text{AR}}$ (token shifting) for all $j \leq N-1$ and determine ϵ_j via matrix inversion. Substituting these back into Eq. 2 yields the final ARMA attention output $\boldsymbol{o}_t^{\text{AR}} + \boldsymbol{o}_t^{\text{MA}}$ for step t.

However, computing $\boldsymbol{o}_t^{\text{MA}}$ requires inverting $\mathbf{I} + \mathbf{\Theta}$, which involves calculating all $\boldsymbol{\theta}_{t-1,j}$ in the $N \times N$ matrix. This increases the complexity of linear attentions back to $O(N^2)$ and may also cause training instability. To maintain linear time complexity, we need a method to compute $\boldsymbol{o}_t^{\text{MA}}$ without explicitly calculating all $\boldsymbol{\theta}_{t-1,j}$ values.

2.6 Indirect MA weight generation

We need an approach that can leverage linear attention's efficiency to compute $\boldsymbol{o}_t^{\text{MA}}$ without the costly $\mathbf{\Theta}^{N\times N}$ matrix operations. Instead of separately calculating attention weights to determine $\boldsymbol{\epsilon_j}$ as value input and recomputing the whole MA output, we aim to use a linear RNN to collect all keys and values at once. We observe from Eq. 3 that there is already a sequential relationship between $\boldsymbol{r}_j$ and $\boldsymbol{\epsilon}_j$, and $\boldsymbol{r}_j$ can be computed directly once $\boldsymbol{o}_t^{\text{AR}}$ is determined. Therefore, we implicitly compute the MA weights of $\boldsymbol{\epsilon_j}$ by using $\boldsymbol{r}_j$ as value input for the MA component instead of $\boldsymbol{\epsilon}_j$. Let $\boldsymbol{\beta}_{t-1,j}$ denote the generated attention weights corresponding to $\boldsymbol{r}_j$ at step t, and let $\boldsymbol{\theta}_{t-1,j}$ here be the implicit MA weights hiddenly linked to the generated $\boldsymbol{\beta}_{t-1,j}$. Based on Eq. 3, we establish:

$$\sum_{j=1}^{t-1} \boldsymbol{\beta}_{t-1,j} \odot \boldsymbol{r}_j = \sum_{j=1}^{t-1} \boldsymbol{\theta}_{t-1,j} \odot \boldsymbol{\epsilon}_j \Leftrightarrow \mathbf{Br} = \mathbf{\Theta}\epsilon \;\; \text{(for one channel)} \tag{4}$$
$$\mathbf{B} = \mathbf{\Theta} \cdot (\mathbf{I} + \mathbf{\Theta})^{-1}, \;\; \mathbf{\Theta} = \mathbf{B} \cdot (\mathbf{I} - \mathbf{B})^{-1}$$

With $\mathbf{\Theta} = \mathbf{B} \cdot (\mathbf{I} - \mathbf{B})^{-1}$, as long as the indirectly generated $\mathbf{\Theta}$ accurately reflects the characteristics of the MA weights we want, we can use $\sum_{j=1}^{t-1} \boldsymbol{\beta}_{t-1,j} \odot \boldsymbol{r}_j$ as $\boldsymbol{o}_t^{\text{MA}}$. Since $\boldsymbol{r}_j$ is known after computing $\boldsymbol{o}_t^{\text{AR}}$, linear attention can be used to compute $\boldsymbol{o}_t^{\text{MA}}$ without increasing the time complexity. To ensure the implicitly generated $\mathbf{\Theta}$ from $\mathbf{B}$ captures the desired MA properties, we must carefully design how $\mathbf{B}$ is generated. The invertibility of $(\mathbf{I} - \mathbf{B})^{-1}$ is guaranteed since $\mathbf{B}$ is strictly lower triangular. To efficiently compute the generated weights, we use the $\boldsymbol{\beta}_{t-1,j} = \phi_q^{\text{MA}}(\boldsymbol{q}_{t-1}^{\text{MA}})\phi_k^{\text{MA}}(\boldsymbol{k}_j^{\text{MA}})$ to generate $\mathbf{B}$, similar to linear attention. Previous dynamic ARMA models in statistics often update MA weights based on observations (Grenier, 1983; Azrak & Mélard, 2006), so we derive $\boldsymbol{q}_{t-1}^{\text{MA}}$ and $\boldsymbol{k}_j^{\text{MA}}$ by multiplying the attention input $\boldsymbol{x}_\cdot$ with $\mathbf{W}_q^{\text{MA}}$ and $\mathbf{W}_k^{\text{MA}}$. Now, the effectiveness of MA weights lies in selecting the most suitable functions $\phi_q^{\text{MA}}(\cdot)$ and $\phi_k^{\text{MA}}(\cdot)$.

2.7 Selection of $\phi(\cdot)$ and characteristics of implicit MA weights

The MA term models short-term effects and local temporal relationships, so we want the implicit $\mathbf{\Theta}$ to follow a pattern where elements near the diagonal have larger absolute values, and those farther away gradually decrease. The expanded form of $\mathbf{\Theta}$ is given by $\mathbf{\Theta} = \mathbf{B} \cdot (\mathbf{I} - \mathbf{B})^{-1} = \mathbf{B} + \mathbf{B}^2 + \mathbf{B}^3 + \cdots$. The elements along the diagonal direction in $\mathbf{B}$ continually accumulate as products into the elements below them in $\mathbf{\Theta}$. Since $\mathbf{B}$ is strictly lower triangular, the elements of the subdiagonal in $\mathbf{\Theta}$ remain constant, while the elements further down progressively accumulate additional terms formed by the product of different $\beta_\cdot$ elements above. Assuming $\beta_\cdot$ follows a distribution and simplifying by setting each $\beta_\cdot$ to the distribution mean b, the elements of $\mathbf{\Theta}$ can be expressed as:

$$\theta_{ij} = b(1+b)^{i-j-1}, \quad \text{where } i > j \tag{5}$$

This simplification offers valuable insights. To prevent longer-term errors from having a larger impact, we aim to avoid large absolute values accumulating in $\mathbf{\Theta}$ far from the diagonal. We also want $\theta_{\cdot}$ to decay steadily as it moves away from the diagonal. Therefore, constraining $\beta_{\cdot}$ between -1 and 0, with a preference of smaller absolute values, is a practical approach.

We tested various activation function combinations for $\phi_q^{\text{MA}}(\cdot)$ and $\phi_k^{\text{MA}}(\cdot)$ to generate $\boldsymbol{\beta}_{t-1,j} = \phi_q^{\text{MA}}(\boldsymbol{q}_{t-1}^{\text{MA}})\phi_k^{\text{MA}}(\boldsymbol{k}_j^{\text{MA}})$ values, as shown in Fig. 4, 7, and 8. We used the sigmoid function $\phi_k^{\text{MA}}(\boldsymbol{k}_j^{\text{MA}}) = \sigma(\alpha \boldsymbol{k}_j^{\text{MA}}/\sqrt{d})$ to obtain values between 0 and 1, where $\alpha = 0.05$ [1] and $\sqrt{d}$ are scaling factors to maintain small absolute values. Then, we selected a function $\phi_q^{\text{MA}}(\cdot)$ to make the product negative. We ultimately chose $\phi_q^{\text{MA}}(\boldsymbol{q}_t^{\text{MA}}) = -\text{LeakyReLU}(-\boldsymbol{q}_t^{\text{MA}}/\sqrt{d})$ with a negative slope of 0.02. The inner negative sign maintains directional consistency (for later parameter sharing), and the outer negative sign encourages a negative output.

Fig. 4 shows that LeakyReLU provides a balanced lag weight pattern. Unlike ReLU and Sigmoid, which only output values of the same sign, LeakyReLU offers some relaxation while keeping most values negative. This adds flexibility by enabling the desired negative smoothing effect of the MA term, with occasional positive values to enhance modeling flexibility.

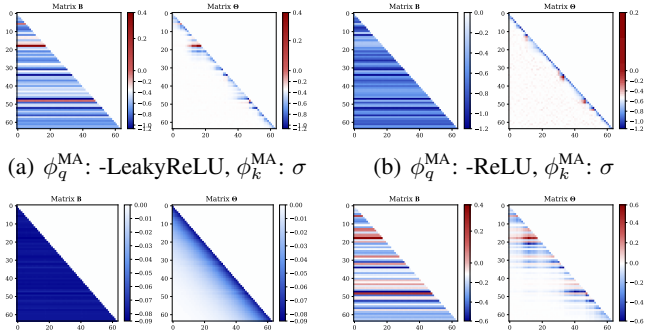

(a) ϕ_q^{MA}: -LeakyReLU, ϕ_k^{MA}: σ (b) ϕ_q^{MA}: -ReLU, ϕ_k^{MA}: σ

(c) ϕ_q^{MA}: -σ, ϕ_k^{MA}: σ (d) ϕ_q^{MA}: -Swish, ϕ_k^{MA}: σ

Figure 4: Visualization of the $\mathbf{B}$(left) $-$ $\mathbf{\Theta}$(right) relationship with different $\phi(\cdot)$. We construct the simulated $\mathbf{B}$ matrices using randomly sampled $\boldsymbol{q}$ and $\boldsymbol{k}$ ($N = 64$, $d = 32$) from the normal distribution, and display the corresponding implicit $\mathbf{\Theta}$ matrices.

To summarize the ARMA attention process with indirect MA weight generation: First, we compute all $\boldsymbol{o}_t^{\text{AR}}$ using the selected attention mechanism. Then, we apply token shifting and compute all $\boldsymbol{r}_j$ for $j \leq N-1$. Next, using $\phi_q^{\text{MA}}(\boldsymbol{q}_t^{\text{MA}})$, $\phi_k^{\text{MA}}(\boldsymbol{k}_j^{\text{MA}})$, and $\boldsymbol{r}_j$, we calculate $\boldsymbol{o}_t^{\text{MA}}$ with the efficient method matching AR attention, as illustrated in Fig. 3. Finally, the ARMA output is $\boldsymbol{o}_t = (\boldsymbol{o}_t^{\text{AR}} + \boldsymbol{o}_t^{\text{MA}})\mathbf{W}_o$. A summary of MA computation methods for each attention mechanism is in Table 1.

Computational cost and model performance The introduction of MA term adds three weight matrices $\mathbf{W}_{\{q,k,v\}}^{\text{MA}}$, increasing parameter size. To ensure fair comparison, we use weight-sharing to match the parameter sizes of ARMA and AR models. Specifically, we share $\mathbf{W}_q$ between the AR and MA terms and set $\mathbf{W}_v$ to an identity matrix, with minimal impact due to the existance of $\mathbf{W}_o$ and the MLP layer (see Eq. 1). This reduces ARMA's trainable weights to $\mathbf{W}_q, \mathbf{W}_k^{\text{AR}}, \mathbf{W}_k^{\text{MA}}, \mathbf{W}_o$, as shown in Fig. 3. While ARMA attention has the same time complexity in order of magnitude as efficient AR attention, its two-stage structure may increase computational costs on constant level. We compare models with different number of layer in the experiements section to show that ARMA's improved performance is due to structural enhancements, but not increased complexity.

3 Experiments

We conducted comprehensive experiments on 12 widely-used TSF datasets, including Weather, Solar, Electricity (ECL), ETTs, Traffic, and PEMS. See §A.1 for detailed description of datasets.

Baselines We built AR Transformers using the five attention mechanisms from Table 1 and added MA terms to create ARMA attention for comparison in TSF tasks. Additionally, we included five

[1] In the key activation, α controls the variance of each row in the $\mathbf{B}$ matrix, indirectly influencing the amount of long-term information (lower left) in the MA weights $\mathbf{\Theta}$. Increasing α would make the MA weights focus more on modeling long-term information. However, since we want the AR weights to handle the long-term component, we set α to a relatively small value. This explains why the rows of the $\mathbf{B}$ matrix appear smooth in the visualization. Refer to Fig. 7 for more details on α, and see Fig. 8 for the effects of reversed positive ϕ_q.

Table 1: Summary of ARMA attention for various attention mechanisms, detailing the calculation methods for AR output and MA output, where $\boldsymbol{r}_j = \boldsymbol{v}_{j+1} - \boldsymbol{o}_j^{\text{AR}}$.

Model	AR term output $\boldsymbol{o}_t^{\text{AR}}$	Indirect MA term output $\boldsymbol{o}_t^{\text{MA}}$
Standard Softmax Attention (Std Attn)	$\frac{\sum_{i=1}^{t} \exp(\boldsymbol{q}_t(\boldsymbol{k}_i^{\text{AR}})^\top)\boldsymbol{v}_i}{\sum_{i=1}^{t} \exp(\boldsymbol{q}_t(\boldsymbol{k}_i^{\text{AR}})^\top)}$	$\sum_{j=1}^{t-1} \phi_q^{\text{MA}}(\boldsymbol{q}_{t-1})\phi_k^{\text{MA}}(\boldsymbol{k}_j^{\text{MA}})^\top \boldsymbol{r}_j$
Linear Attention (Lin Attn)	$\boldsymbol{q}_t \sum_{i=1}^{t} (\boldsymbol{k}_i^{\text{AR}})^\top \boldsymbol{v}_i$	$\phi_q^{\text{MA}}(\boldsymbol{q}_{t-1}) \sum_{j=1}^{t-1} \phi_k^{\text{MA}}(\boldsymbol{k}_j^{\text{MA}})^\top \boldsymbol{r}_j$
Element-wise Linear Attention (ELin Attn)	$\sigma(\boldsymbol{q}_t) \odot \frac{\sum_{i=1}^{t} \exp(\boldsymbol{k}_i^{\text{AR}}) \odot \boldsymbol{v}_i}{\sum_{i=1}^{t} \exp(\boldsymbol{k}_i^{\text{AR}})}$	$\phi_q^{\text{MA}}(\boldsymbol{q}_{t-1}) \odot \sum_{j=1}^{t-1} \phi_k^{\text{MA}}(\boldsymbol{k}_j^{\text{MA}}) \odot \boldsymbol{r}_j$
Gated Linear Attention (GLin Attn)	$\boldsymbol{q}_t \sum_{i=1}^{t} \mathbf{G}_i \odot (\boldsymbol{k}_i^{\text{AR}})^\top \boldsymbol{v}_i$	$\phi_q^{\text{MA}}(\boldsymbol{q}_{t-1}) \sum_{j=1}^{t-1} \phi_k^{\text{MA}}(\boldsymbol{k}_j^{\text{MA}})^\top \boldsymbol{r}_j$
Fixed Attention (Fixed Attn)	$\sum_{i=1}^{t} w_{t,i}^{\text{AR}} \boldsymbol{v}_i$	$\phi_q^{\text{MA}}(\boldsymbol{w}_{t-1}^{\text{MA,q}}) \sum_{j=1}^{t-1} \phi_k^{\text{MA}}(\boldsymbol{w}_j^{\text{MA,k}})^\top \boldsymbol{r}_j$

recent SOTA baselines: FITS (Xu et al., 2024), iTransformer (Liu et al., 2024a), CATS (Lu et al., 2024), PatchTST (Nie et al., 2022), and DLinear (Zeng et al., 2023). We also used a simple channel-dependent encoder-only Transformer, modified by repeating the last input value (like NLinear) to address distribution shift. This model already surpasses older architectures like Autoformer (Wu et al., 2021) and Informer (Zhou et al., 2021), so we excluded these from our comparison.

In the main experiments, both AR and ARMA Transformers use a consistent setup: $m = 3$ Transformer layers, 8 heads, and model dimension determined by a empirical method $d = 16\sqrt{C}$, where C is the number of series. We evaluate their performance using one-step prediction for each test datapoint, aligned with the baselines. Baseline hyperparameters are set to the reported values from their original papers. For more details on hyperparameters and implementation, see §A.2.

L_I, L_P, and fair comparison AR/ARMA Transformers maintain stable performance across different input lengths L_I and forecasting horizons L_P. In the main experiments, we set $L_I = 512$ and test with $L_P \in \{12, 24, 48, 96\}$. We did not select longer L_P values for the **main experiments** because the token length in our AR/ARMA Transformer is determined by L_I/L_P. For longer horizons like $L_P = 720$, AR/ARMA Transformers need a larger L_I (e.g., 4096). If $L_I = 512$ is used, it results in only one token, reducing the model to a simple MLP, which is feasible but fails to demonstrate the strengths of the AR/ARMA structure. However, increasing L_I for baselines would hurt their performance, as $L_I = 512$ is within the optimal range for them. To ensure fairness, we use these settings for the main experiments and later include additional experiments extending L_I to 4096 and L_P to 720.

We ran all models on all datasets for the four different L_P. In the main text, we report the average test set MSE for each model across different L_P on each dataset and provide the full results in §A.3.

Main TSF results Table 2 highlights the significant performance gains from extending AR Transformers to the ARMA structure. All ARMA attention mechanisms outperform their AR counterparts in both average test MSE and ranking, with linear and standard attention showing the best results.

Performance of linear attention Linear attention outperforms softmax attention in TSF, suggesting that simpler attention patterns and non-normalized input shortcuts (without denominator) can improve generalization on time-varying distributions. This aligns with earlier findings where linear models can outperform more complex Transformers in TSF (Zeng et al., 2023; Xu et al., 2024).

Performance of gated linear attention ARMA brought the greatest improvement to gated linear attention. In gated AR models, the decay factor helps the AR term focus on important local patterns, but it weakens the ability to capture long-term or stable cyclic patterns. By introducing the MA term, local effects are absorbed, allowing the decay factor to function properly in the AR forgetting mechanism, leading to significant performance gains.

Performance of fixed attention Fixed attention, which lacks dynamic parameter generation, performs worse than other attention. However, its significant improvement with MA terms shows that ARMA enhances the model's ability structurally to capture comprehensive sequence patterns.

Performance and complexity The improvement of adding the MA term comes from its ability to model short-term impacts, allowing the AR term to focus on long-term and cyclic effects, not from

Table 2: Summary of main TSF results with forecasting horizons $L_P \in \{12, 24, 48, 96\}$ and $L_I = 512$. See Table 8 for the original results. Averages of test set MSE for each model on each dataset are presented. Average rankings (AvgRank) of each model, along with the count of first-place rankings (#Top1), are also included. Green indicates better performance, while red indicates worse. For each comparison between AR and ARMA attention, the better model is underlined.

Model	AR/ARMA Transformer										Baseline					
	Std Attn	Std Attn +ARMA	Lin Attn	Lin Attn +ARMA	GLin Attn	GLin Attn +ARMA	ELin Attn	ELin Attn +ARMA	Fixed Attn	Fixed Attn +ARMA	FITS	iTrans-former	CATS	PatchTST	DLinear	Enc-Former
Weather	0.104	0.101	0.104	0.100	0.119	0.105	0.104	0.103	0.105	0.104	0.114	0.117	0.105	0.107	0.124	0.135
Solar	0.134	0.124	0.122	0.119	0.148	0.124	0.136	0.133	0.142	0.135	0.152	0.145	0.122	0.150	0.149	0.125
ECL	0.110	0.106	0.106	0.104	0.110	0.108	0.115	0.114	0.121	0.118	0.124	0.106	0.110	0.111	0.114	0.201
ETTh1	0.323	0.318	0.318	0.316	0.408	0.321	0.323	0.321	0.330	0.328	0.333	0.351	0.327	0.335	0.329	0.817
ETTh2	0.192	0.192	0.193	0.195	0.217	0.198	0.193	0.190	0.200	0.194	0.197	0.229	0.194	0.201	0.198	0.597
ETTm1	0.264	0.239	0.238	0.222	0.407	0.260	0.246	0.244	0.267	0.251	0.237	0.259	0.222	0.244	0.235	0.429
ETTm2	0.131	0.128	0.126	0.121	0.142	0.128	0.134	0.128	0.129	0.127	0.115	0.135	0.116	0.119	0.120	0.311
Traffic	0.341	0.333	0.337	0.330	0.429	0.350	0.352	0.348	0.373	0.365	0.385	0.330	0.372	0.358	0.375	0.847
PEMS03	0.112	0.100	0.100	0.096	0.209	0.101	0.116	0.112	0.121	0.116	0.133	0.096	0.105	0.140	0.134	0.111
PEMS04	0.118	0.106	0.103	0.098	0.167	0.105	0.122	0.119	0.128	0.124	0.151	0.098	0.108	0.164	0.148	0.099
PEMS07	0.092	0.083	0.087	0.077	0.093	0.087	0.101	0.097	0.106	0.100	0.132	0.079	0.094	0.093	0.129	0.102
PEMS08	0.148	0.132	0.119	0.116	0.159	0.125	0.150	0.144	0.161	0.152	0.201	0.117	0.135	0.121	0.193	0.183
AvgRank	7.958	4.292	4.271	2.333	12.375	6.229	8.938	7.125	11.146	8.688	12.042	7.271	5.938	9.792	11.250	12.813
#Top1	0	4	4	25	0	1	1	3	1	3	0	5	4	1	2	4

Table 3: Summary showing that ARMA Transformers with $m = 3$ layers consistently outperform their AR counterparts across a wide range of m. The same experimental settings and data presentation method as in Table 2 are used. See Table 9 for the original results.

	Model	$m = 3$ ARMA	$m = 1$ AR	$m = 2$ AR	$m = 3$ AR	$m = 4$ AR	$m = 5$ AR	$m = 6$ AR	$m = 7$ AR	$m = 8$ AR
Weather	Std Attn	0.101	0.109	0.108	0.104	0.108	0.113	0.111	0.113	0.112
	Lin Attn	0.100	0.104	0.103	0.104	0.103	0.103	0.103	0.102	0.103
	GLin Attn	0.105	0.122	0.122	0.119	0.121	0.121	0.122	0.121	0.120
	ELin Attn	0.103	0.110	0.107	0.104	0.108	0.109	0.111	0.110	0.111
	Fixed Attn	0.104	0.113	0.109	0.105	0.110	0.112	0.110	0.110	0.110
ETTm1	Std Attn	0.239	0.265	0.270	0.264	0.266	0.269	0.270	0.270	0.272
	Lin Attn	0.222	0.241	0.233	0.238	0.232	0.230	0.230	0.231	0.231
	GLin Attn	0.260	0.411	0.413	0.407	0.409	0.410	0.410	0.409	0.404
	ELin Attn	0.244	0.253	0.251	0.246	0.253	0.257	0.259	0.256	0.258
	Fixed Attn	0.251	0.269	0.264	0.267	0.260	0.258	0.259	0.258	0.257

increased computational costs. Table 3 shows that, regardless of the number of layers m (1 to 8), AR Transformers consistently underperform compared to ARMA Transformers with a fixed $m = 3$.

Table 4: Summary showing that AR/ARMA Transformers effectively utilize extended lookback L_I, while baselines experience performance degradation. $L_I \in \{512, 1024, 2048, 4096\}$ with $L_P \in \{12, 24, 48, 96\}$ are evaluated and averaged. Original results can be found in Table 10.

	Model	AR/ARMA Transformer										Baseline					
		Std Attn	Std Attn +ARMA	Lin Attn	Lin Attn +ARMA	GLin Attn	GLin Attn +ARMA	ELin Attn	ELin Attn +ARMA	Fixed Attn	Fixed Attn +ARMA	FITS	iTrans-former	CATS	PatchTST	DLinear	Enc-Former
Weather	$L_I = 512$	0.104	0.101	0.104	0.100	0.119	0.105	0.104	0.103	0.105	0.104	0.114	0.117	0.105	0.108	0.124	0.135
	$L_I = 1024$	0.107	0.102	0.102	0.101	0.116	0.104	0.106	0.106	0.108	0.105	0.120	0.117	0.108	0.120	0.118	0.124
	$L_I = 2048$	0.110	0.102	0.101	0.100	0.114	0.102	0.108	0.108	0.123	0.110	0.121	0.119	0.113	0.122	0.119	0.128
	$L_I = 4096$	0.108	0.102	0.100	0.100	0.115	0.105	0.109	0.107	0.110	0.108	0.124	0.132	0.123	0.125	0.121	0.136
ETTm1	$L_I = 512$	0.264	0.239	0.238	0.222	0.407	0.260	0.246	0.244	0.267	0.251	0.237	0.259	0.222	0.244	0.235	0.429
	$L_I = 1024$	0.280	0.241	0.239	0.227	0.423	0.236	0.265	0.253	0.281	0.263	0.240	0.258	0.238	0.245	0.239	0.364
	$L_I = 2048$	0.278	0.239	0.233	0.223	0.327	0.232	0.281	0.252	0.288	0.268	0.246	0.248	0.261	0.250	0.239	0.415
	$L_I = 4096$	0.275	0.234	0.237	0.226	0.324	0.229	0.282	0.265	0.287	0.266	0.252	0.274	0.340	0.260	0.250	0.428

Adaptability to Longer L_I Previous baseline models typically use L_I between 96 and 720, as longer L_I often leads to overfitting to long-term patterns, ignoring more important local effects (Zeng et al., 2023; Nie et al., 2022; Liu et al., 2024a). However, the next-step prediction and varying lookback inputs in AR/ARMA Transformers help the model focus on tokens closer to the next step, improving generalization. As shown in Table 4, increasing L_I from 512 to 4096 improves AR/ARMA performance, demonstrating scalability and the ability to properly leverage long-term effects. Also, the ARMA structure consistently boosts AR model performance across different L_I.

Varying L_P We evaluated AR/ARMA Transformers with $L_I = 4096$ on long-term output $L_P = 720$ while keeping the best-performing $L_I = 512$ for the baselines. We also compared short-term output with $L_P = 1$ using $L_I = 512$ for all models. As shown in Table 5, across different L_P, AR models performed comparably to baselines, and the ARMA structure consistently improved performance over AR models.

Comparison to MEGA The MEGA structure (Ma et al., 2022) uses an exponential moving average (EMA) in gated attention to model local patterns. However, applying EMA directly to AR weights weakens the model's ability to capture long-term and stable seasonal patterns, making it less effective than ARMA at decoupling long-term and short-term effects. Table 6 shows that the performance of using MEGA as the attention mechanism is similar to using gated linear attention without the MA term. It provides less improvement compared to gated linear attention with ARMA.

Table 5: Summary of model performance on varying horizons L_P. AR/ARMA Transformers uses $L_I = 512$ for $L_P = 1$ and $L_I = 4096$ for $L_P = 720$. Baselines are consistently set to their best-performing $L_I = 512$ configuration. Original results can be found in Table 11.

Model		AR/ARMA Transformer										Baseline					
		Std Attn	Std Attn +ARMA	Lin Attn	Lin Attn +ARMA	GLin Attn	GLin Attn +ARMA	ELin Attn	ELin Attn +ARMA	Fixed Attn	Fixed Attn +ARMA	FITS	iTrans-former	CATS	PatchTST	DLinear	Enc-Former
Weather	$L_P = 1$	0.037	0.032	0.032	0.031	0.033	0.031	0.037	0.034	0.036	0.034	0.038	0.038	0.033	0.035	0.034	0.032
	$L_P = 720$	0.299	0.301	0.308	0.305	0.310	0.299	0.296	0.295	0.299	0.297	0.327	0.317	0.311	0.325	0.319	0.404
ETTm1	$L_P = 1$	0.048	0.043	0.042	0.041	0.051	0.043	0.053	0.051	0.054	0.052	0.047	0.049	0.043	0.046	0.044	0.044
	$L_P = 720$	0.396	0.391	0.417	0.408	0.396	0.393	0.395	0.391	0.403	0.399	0.420	0.438	0.418	0.408	0.420	0.802
ETTm2	$L_P = 1$	0.034	0.031	0.032	0.030	0.033	0.030	0.035	0.033	0.033	0.031	0.034	0.034	0.032	0.033	0.031	0.035
	$L_P = 720$	0.329	0.327	0.341	0.338	0.334	0.328	0.327	0.326	0.331	0.327	0.360	0.369	0.351	0.362	0.403	2.641

Table 6: Summary of the performance comparison with MEGA. See Table 12 for the original result.

Model	Std Attn	Std Attn +ARMA	Lin Attn	Lin Attn +ARMA	GLin Attn	GLin Attn +ARMA	MEGA
Weather	0.104	0.101	0.104	0.100	0.119	0.105	0.121
Solar	0.134	0.124	0.122	0.119	0.148	0.124	0.226
ETTh1	0.323	0.318	0.318	0.316	0.408	0.321	0.404
ETTh2	0.192	0.192	0.193	0.195	0.217	0.198	0.214
ETTm1	0.264	0.239	0.238	0.222	0.407	0.260	0.412
ETTm2	0.131	0.128	0.126	0.121	0.142	0.128	0.137
PEMS03	0.112	0.100	0.100	0.096	0.209	0.101	0.161

Visualization analysis Fig. 5 shows test loss curves for different AR/ARMA attention mechanisms on the Weather and ETTm1 datasets, with ARMA consistently outperforming AR in both convergence speed and final loss. Fig. 6 visualizes attention input sequence, AR weights, $\mathbf{B}$, and $\mathbf{\Theta}$ matrices of a test datapoint on Weather, showing how MA weights decouple local patterns, allowing AR weights to focus on cyclic and long-term patterns. Additional visualizations in Figs. 9–12 reinforce that there are important long-term stable seasonal patterns for AR weights to capture that should not be disrupted by applying forget gates or EMA. This explains why gated linear attention underperforms linear attention in our experiments.

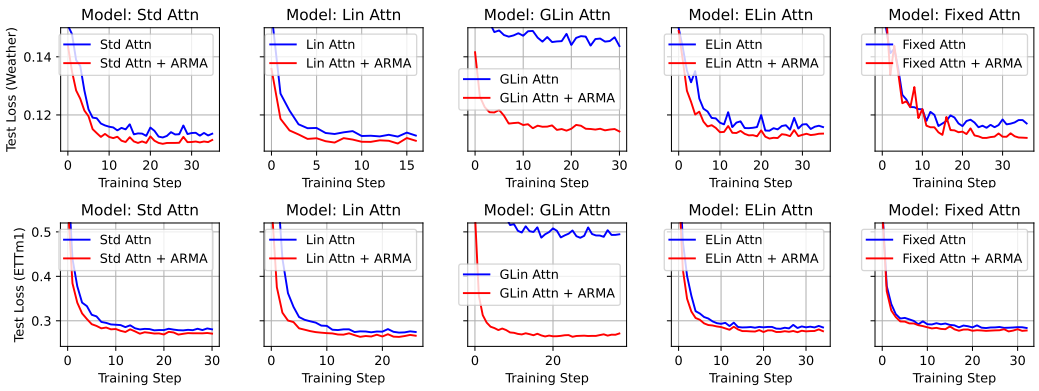

Figure 5: Visualization of test loss curves. We show the testing performance of five attention mechanisms using AR/ARMA structures on the Weather and ETTm1 datasets ($L_I = 512$, $L_P = 48$).

Computational cost Table 7 compares the computational cost of AR/ARMA Transformers with baselines on the ETTm1 dataset. Our tokenization method reduces the token size N, keeping AR/ARMA models' computational cost comparable to the baselines. Additionally, parameter sharing ensures the MA term doesn't increase the number of parameters, and the extra FLOPs from using ARMA are not significant.

4 Related Works

Linear attention with exponential moving-average Beyond using a gating decay factor on the hidden state matrix of linear attention (Mao, 2022; Sun et al., 2023; Yang et al., 2024), recent studies have explored incorporating EMA mechanisms into gated linear attention by applying a smoothing factor (summing to 1) to the two terms in the state update (Ma et al., 2022). Similar EMA mechanisms have also been used in many modern RNN structures (Gu et al., 2022; Peng et al., 2023; Orvieto et al., 2023; Qin et al., 2024). Additionally, Schiele et al. (2022) attempted to introduce the ARMA structure into traditional RNNs, but their method could not ensure that the generated MA

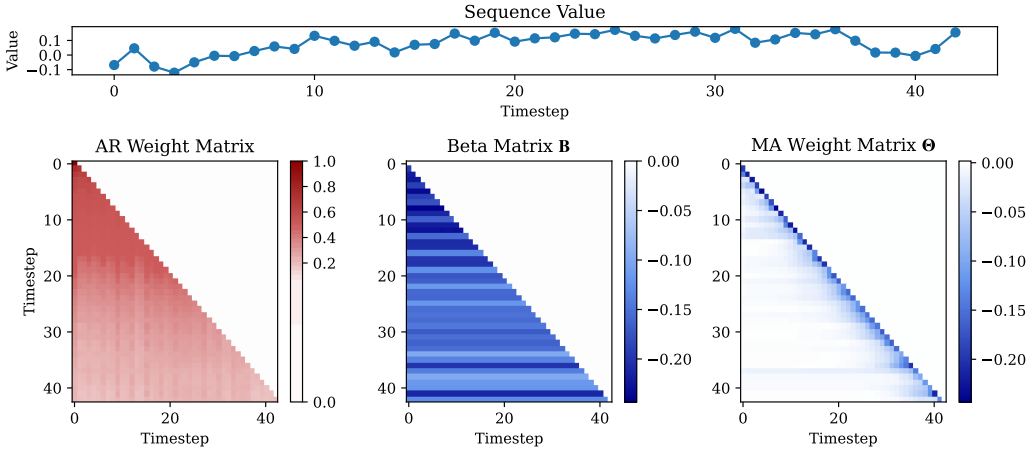

Figure 6: Visualization of the ARMA attention weights (first attention layer, averaged across the multiple heads or d-dimensional channels) for the first test set data point in the Weather dataset ($L_I = 4096$, $L_P = 96$). More ARMA weight visualization can be found in Fig. 9, 10, 11, and 12.

Table 7: Comparison of computational costs utilizing the data format of ETTm1 to build model inputs ($L_I = 512$). The hyper-parameters for models are set according to their default configurations.

Models	EncFormer		CATS		PatchTST		iTransformer		DLinear		FITS	
Metric	FLOPs	Params	FLOPs	Params	FLOPs	Params	FLOPs	Params	FLOPs	Params	FLOPs	Params
$L_P = 96$	1.442G	1.646M	262.9M	1.326M	180.9M	1.046M	81.96M	1.857M	4.337M	98.50K	334.0K	24.02K
$L_P = 48$	1.328G	1.646M	243.5M	1.227M	163.6M	652.9K	81.69M	1.851M	2.174M	49.25K	308.1K	22.16K
$L_P = 24$	1.271G	1.645M	233.9M	1.178M	155.0M	456.3K	81.56M	1.848M	1.093M	24.62K	294.2K	21.16K
$L_P = 12$	1.242G	1.645M	229.0M	1.154M	150.7M	358.0K	81.49M	1.847M	552.5K	12.31K	288.3K	20.74K
Model	GLin Attn		GLin Attn +ARMA		Lin Attn		Lin Attn +ARMA		ELin Attn		ELin Attn +ARMA	
Metric	FLOPs	Params	FLOPs	Params	FLOPs	Params	FLOPs	Params	FLOPs	Params	FLOPs	Params
$L_P = 96$	7.403M	45.81K	7.431M	45.81K	7.387M	45.79K	7.415M	45.79K	7.258M	45.79K	7.266M	45.79K
$L_P = 48$	12.63M	43.97K	12.77M	43.97K	12.60M	43.95K	12.74M	43.95K	12.36M	43.95K	12.37M	43.95K
$L_P = 24$	24.30M	45.22K	24.70M	45.22K	24.25M	45.21K	24.64M	45.21K	23.77M	45.21K	23.80M	45.21K
$L_P = 12$	46.58M	49.82K	47.45M	49.82K	46.46M	49.80K	47.34M	49.80K	45.54M	49.80K	45.60M	49.80K

weights can properly model short-term patterns, and the final results did not significantly surpass traditional RNNs nor compare with recent attention models.

TSF Structures The use of neural network structures for TSF has been widely explored (Hochreiter & Schmidhuber, 1997; Rangapuram et al., 2018; Salinas et al., 2020). Recently, many Transformer-based TSF models with encoder-only and encoder-decoder structures have emerged (Li et al., 2019a; Zhou et al., 2021; Wu et al., 2021; Zhang & Yan, 2023; Nie et al., 2022; Liu et al., 2024a). However, these complex Transformer architectures have not significantly outperformed simpler MLP or linear models (Zeng et al., 2023; Das et al., 2023; Xu et al., 2024; Lu et al., 2024). Additionally, these models struggle to handle short-term effects properly with longer lookback windows, where, paradoxically, longer inputs often lead to worse performance.

5 Conclusion, Limitation, and Future Works

We propose the ARMA attention mechanism, which integrates an MA term into existing AR attention using a novel indirect MA weight generation method. This approach maintains the same time complexity and parameter size while ensuring the validity of the implicit MA weights. Experiments demonstrate that ARMA attention successfully decouples and handles long-term and short-term effects. The ARMA Transformer, enhanced with the MA term, outperforms their AR counterparts and achieves state-of-the-art results, offering consistent improvements in training with minimal added computational cost.

One limitation is that we have not explored combining the channel-independent ARMA Transformer with multivariate forecasting models to improve its handling of inter-series relationships. For future work, ARMA attention could be applied to general sequence modeling tasks beyond TSF. Testing on larger-scale datasets, such as using ARMA Transformers for large-scale NLP pretraining, is another promising direction.

REFERENCES

Rajae Azrak and Guy Mélard. Asymptotic properties of quasi-maximum likelihood estimators for arma models with time-dependent coefficients. *Statistical Inference for Stochastic Processes*, 9: 279–330, 2006.

Zalán Borsos, Raphaël Marinier, Damien Vincent, Eugene Kharitonov, Olivier Pietquin, Matt Sharifi, Dominik Roblek, Olivier Teboul, David Grangier, Marco Tagliasacchi, et al. Audiolm: a language modeling approach to audio generation. *IEEE/ACM transactions on audio, speech, and language processing*, 31:2523–2533, 2023.

George EP Box, Gwilym M Jenkins, and John F MacGregor. Some recent advances in forecasting and control. *Journal of the Royal Statistical Society: Series C (Applied Statistics)*, 23(2):158–179, 1974.

Tom Brown, Benjamin Mann, Nick Ryder, Melanie Subbiah, Jared D Kaplan, Prafulla Dhariwal, Arvind Neelakantan, Pranav Shyam, Girish Sastry, Amanda Askell, Sandhini Agarwal, Ariel Herbert-Voss, Gretchen Krueger, Tom Henighan, Rewon Child, Aditya Ramesh, Daniel Ziegler, Jeffrey Wu, Clemens Winter, Chris Hesse, Mark Chen, Eric Sigler, Mateusz Litwin, Scott Gray, Benjamin Chess, Jack Clark, Christopher Berner, Sam McCandlish, Alec Radford, Ilya Sutskever, and Dario Amodei. Language models are few-shot learners. In H. Larochelle, M. Ranzato, R. Hadsell, M.F. Balcan, and H. Lin (eds.), *Advances in Neural Information Processing Systems*, volume 33, pp. 1877–1901. Curran Associates, Inc., 2020. URL https://proceedings.neurips.cc/paper_files/paper/2020/file/1457c0d6bfcb4967418bfb8ac142f64a-Paper.pdf.

Huiwen Chang, Han Zhang, Lu Jiang, Ce Liu, and William T Freeman. Maskgit: Masked generative image transformer. In *Proceedings of the IEEE/CVF Conference on Computer Vision and Pattern Recognition*, pp. 11315–11325, 2022.

Mark Chen, Alec Radford, Rewon Child, Jeffrey Wu, Heewoo Jun, David Luan, and Ilya Sutskever. Generative pretraining from pixels. In *International conference on machine learning*, pp. 1691–1703. PMLR, 2020.

Krzysztof Marcin Choromanski, Valerii Likhosherstov, David Dohan, Xingyou Song, Andreea Gane, Tamas Sarlos, Peter Hawkins, Jared Quincy Davis, Afroz Mohiuddin, Lukasz Kaiser, David Benjamin Belanger, Lucy J Colwell, and Adrian Weller. Rethinking attention with performers. In *International Conference on Learning Representations*, 2021. URL https://openreview.net/forum?id=Ua6zuk0WRH.

Abhimanyu Das, Weihao Kong, Andrew Leach, Shaan K Mathur, Rajat Sen, and Rose Yu. Long-term forecasting with tiDE: Time-series dense encoder. *Transactions on Machine Learning Research*, 2023. ISSN 2835-8856. URL https://openreview.net/forum?id=pCbC3aQB5W.

Abhimanyu Das, Weihao Kong, Rajat Sen, and Yichen Zhou. A decoder-only foundation model for time-series forecasting. In *Forty-first International Conference on Machine Learning*, 2024. URL https://openreview.net/forum?id=jn2iTJas6h.

Patrick Esser, Robin Rombach, and Bjorn Ommer. Taming transformers for high-resolution image synthesis. In *Proceedings of the IEEE/CVF conference on computer vision and pattern recognition*, pp. 12873–12883, 2021.

Yves Grenier. Time-dependent arma modeling of nonstationary signals. *IEEE Transactions on Acoustics, Speech, and Signal Processing*, 31(4):899–911, 1983.

Nate Gruver, Marc Anton Finzi, Shikai Qiu, and Andrew Gordon Wilson. Large language models are zero-shot time series forecasters. In *Thirty-seventh Conference on Neural Information Processing Systems*, 2023. URL https://openreview.net/forum?id=md68e8iZK1.

Albert Gu, Karan Goel, Ankit Gupta, and Christopher Ré. On the parameterization and initialization of diagonal state space models. In Alice H. Oh, Alekh Agarwal, Danielle Belgrave, and Kyunghyun Cho (eds.), *Advances in Neural Information Processing Systems*, 2022. URL https://openreview.net/forum?id=yJE7iQSAep.

Sepp Hochreiter and Jürgen Schmidhuber. Long short-term memory. *Neural computation*, 9(8): 1735–1780, 1997.

Charles C Holt. Forecasting seasonals and trends by exponentially weighted moving averages. *International journal of forecasting*, 20(1):5–10, 2004.

Weizhe Hua, Zihang Dai, Hanxiao Liu, and Quoc Le. Transformer quality in linear time. In *International conference on machine learning*, pp. 9099–9117. PMLR, 2022.

Ming Jin, Shiyu Wang, Lintao Ma, Zhixuan Chu, James Y. Zhang, Xiaoming Shi, Pin-Yu Chen, Yuxuan Liang, Yuan-Fang Li, Shirui Pan, and Qingsong Wen. Time-LLM: Time series forecasting by reprogramming large language models. In *The Twelfth International Conference on Learning Representations*, 2024. URL https://openreview.net/forum?id=Unb5CVPtae.

Angelos Katharopoulos, Apoorv Vyas, Nikolaos Pappas, and François Fleuret. Transformers are rnns: Fast autoregressive transformers with linear attention. In *International conference on machine learning*, pp. 5156–5165. PMLR, 2020.

Taesung Kim, Jinhee Kim, Yunwon Tae, Cheonbok Park, Jang-Ho Choi, and Jaegul Choo. Reversible instance normalization for accurate time-series forecasting against distribution shift. In *International Conference on Learning Representations*, 2022. URL https://openreview.net/forum?id=cGDAkQo1C0p.

Guokun Lai, Wei-Cheng Chang, Yiming Yang, and Hanxiao Liu. Modeling long- and short-term temporal patterns with deep neural networks. In Kevyn Collins-Thompson, Qiaozhu Mei, Brian D. Davison, Yiqun Liu, and Emine Yilmaz (eds.), *The 41st International ACM SIGIR Conference on Research & Development in Information Retrieval, SIGIR 2018, Ann Arbor, MI, USA, July 08-12, 2018*, pp. 95–104. ACM, 2018. doi: 10.1145/3209978.3210006. URL https://doi.org/10.1145/3209978.3210006.

Shiyang Li, Xiaoyong Jin, Yao Xuan, Xiyou Zhou, Wenhu Chen, Yu-Xiang Wang, and Xifeng Yan. Enhancing the locality and breaking the memory bottleneck of transformer on time series forecasting. *Advances in neural information processing systems*, 32, 2019a.

Shiyang Li, Xiaoyong Jin, Yao Xuan, Xiyou Zhou, Wenhu Chen, Yu-Xiang Wang, and Xifeng Yan. Enhancing the locality and breaking the memory bottleneck of transformer on time series forecasting. *Advances in neural information processing systems*, 32, 2019b.

Yaguang Li, Rose Yu, Cyrus Shahabi, and Yan Liu. Diffusion convolutional recurrent neural network: Data-driven traffic forecasting. *arXiv preprint arXiv:1707.01926*, 2017.

Yong Liu, Tengge Hu, Haoran Zhang, Haixu Wu, Shiyu Wang, Lintao Ma, and Mingsheng Long. itransformer: Inverted transformers are effective for time series forecasting. In *The Twelfth International Conference on Learning Representations*, 2024a. URL https://openreview.net/forum?id=JePfAI8fah.

Yong Liu, Guo Qin, Xiangdong Huang, Jianmin Wang, and Mingsheng Long. Autotimes: Autoregressive time series forecasters via large language models. *arXiv preprint arXiv:2402.02370*, 2024b.

Jiecheng Lu, Xu Han, Yan Sun, and Shihao Yang. Cats: Enhancing multivariate time series forecasting by constructing auxiliary time series as exogenous variables. *arXiv preprint arXiv:2403.01673*, 2024.

Xuezhe Ma, Chunting Zhou, Xiang Kong, Junxian He, Liangke Gui, Graham Neubig, Jonathan May, and Luke Zettlemoyer. Mega: moving average equipped gated attention. *arXiv preprint arXiv:2209.10655*, 2022.

Huanru Henry Mao. Fine-tuning pre-trained transformers into decaying fast weights. In Yoav Goldberg, Zornitsa Kozareva, and Yue Zhang (eds.), *Proceedings of the 2022 Conference on Empirical Methods in Natural Language Processing*, pp. 10236–10242, Abu Dhabi, United Arab Emirates, December 2022. Association for Computational Linguistics. doi: 10.18653/v1/2022.emnlp-main.697. URL https://aclanthology.org/2022.emnlp-main.697.

Yuqi Nie, Nam H Nguyen, Phanwadee Sinthong, and Jayant Kalagnanam. A time series is worth 64 words: Long-term forecasting with transformers. In *The Eleventh International Conference on Learning Representations*, 2022.

Antonio Orvieto, Samuel L Smith, Albert Gu, Anushan Fernando, Caglar Gulcehre, Razvan Pascanu, and Soham De. Resurrecting recurrent neural networks for long sequences. In *International Conference on Machine Learning*, pp. 26670–26698. PMLR, 2023.

Bo Peng, Eric Alcaide, Quentin Anthony, Alon Albalak, Samuel Arcadinho, Stella Biderman, Huanqi Cao, Xin Cheng, Michael Chung, Matteo Grella, et al. Rwkv: Reinventing rnns for the transformer era. *arXiv preprint arXiv:2305.13048*, 2023.

Zhen Qin, Xiaodong Han, Weixuan Sun, Dongxu Li, Lingpeng Kong, Nick Barnes, and Yiran Zhong. The devil in linear transformer. In Yoav Goldberg, Zornitsa Kozareva, and Yue Zhang (eds.), *Proceedings of the 2022 Conference on Empirical Methods in Natural Language Processing*, pp. 7025–7041, Abu Dhabi, United Arab Emirates, December 2022. Association for Computational Linguistics. doi: 10.18653/v1/2022.emnlp-main.473. URL https://aclanthology.org/2022.emnlp-main.473.

Zhen Qin, Songlin Yang, Weixuan Sun, Xuyang Shen, Dong Li, Weigao Sun, and Yiran Zhong. Hgrn2: Gated linear rnns with state expansion. *arXiv preprint arXiv:2404.07904*, 2024.

Alec Radford. Improving language understanding by generative pre-training. *OpenAI technical report*, 2018. URL https://cdn.openai.com/research-covers/language-unsupervised/language_understanding_paper.pdf.

Alec Radford, Jeffrey Wu, Rewon Child, David Luan, Dario Amodei, Ilya Sutskever, et al. Language models are unsupervised multitask learners. *OpenAI blog*, 1(8):9, 2019.

Syama Sundar Rangapuram, Matthias W. Seeger, Jan Gasthaus, Lorenzo Stella, Yuyang Wang, and Tim Januschowski. Deep state space models for time series forecasting. In Samy Bengio, Hanna M. Wallach, Hugo Larochelle, Kristen Grauman, Nicolò Cesa-Bianchi, and Roman Garnett (eds.), *Advances in Neural Information Processing Systems 31: Annual Conference on Neural Information Processing Systems 2018, NeurIPS 2018, December 3-8, 2018, Montréal, Canada*, pp. 7796–7805, 2018. URL https://proceedings.neurips.cc/paper/2018/hash/5cf68969fb67aa6082363a6d4e6468e2-Abstract.html.

David Salinas, Valentin Flunkert, Jan Gasthaus, and Tim Januschowski. Deepar: Probabilistic forecasting with autoregressive recurrent networks. *International Journal of Forecasting*, 36(3):1181–1191, 2020.

Philipp Schiele, Christoph Berninger, and David Rügamer. Arma cell: A modular and effective approach for neural autoregressive modeling. *arXiv preprint arXiv:2208.14919*, 2022.

Yutao Sun, Li Dong, Shaohan Huang, Shuming Ma, Yuqing Xia, Jilong Xue, Jianyong Wang, and Furu Wei. Retentive network: A successor to transformer for large language models. *arXiv preprint arXiv:2307.08621*, 2023.

Hugo Touvron, Thibaut Lavril, Gautier Izacard, Xavier Martinet, Marie-Anne Lachaux, Timothée Lacroix, Baptiste Rozière, Naman Goyal, Eric Hambro, Faisal Azhar, Aurelien Rodriguez, Armand Joulin, Edouard Grave, and Guillaume Lample. Llama: Open and efficient foundation language models, 2023. URL https://arxiv.org/abs/2302.13971.

A Vaswani. Attention is all you need. *Advances in Neural Information Processing Systems*, 2017.

Peter R Winters. Forecasting sales by exponentially weighted moving averages. *Management science*, 6(3):324–342, 1960.

Haixu Wu, Jiehui Xu, Jianmin Wang, and Mingsheng Long. Autoformer: Decomposition transformers with auto-correlation for long-term series forecasting. In Marc'Aurelio Ranzato, Alina Beygelzimer, Yann N. Dauphin, Percy Liang, and Jennifer Wortman Vaughan (eds.), *Advances in Neural Information Processing Systems 34: Annual Conference on Neural Information Processing Systems 2021, NeurIPS 2021, December 6-14, 2021, virtual*, pp. 22419–22430, 2021. URL https://proceedings.neurips.cc/paper/2021/hash/bcc0d400288793e8bdcd7c19a8ac0c2b-Abstract.html.

Zhijian Xu, Ailing Zeng, and Qiang Xu. FITS: Modeling time series with $10k$ parameters. In *The Twelfth International Conference on Learning Representations*, 2024. URL https://openreview.net/forum?id=bWcnvZ3qMb.

Songlin Yang, Bailin Wang, Yikang Shen, Rameswar Panda, and Yoon Kim. Gated linear attention transformers with hardware-efficient training. In *Forty-first International Conference on Machine Learning*, 2024. URL https://openreview.net/forum?id=ia5XvxFUJT.

Ailing Zeng, Muxi Chen, Lei Zhang, and Qiang Xu. Are transformers effective for time series forecasting? In *Proceedings of the AAAI conference on artificial intelligence*, volume 37, pp. 11121–11128, 2023.

Shuangfei Zhai, Walter Talbott, Nitish Srivastava, Chen Huang, Hanlin Goh, Ruixiang Zhang, and Josh Susskind. An attention free transformer. *arXiv preprint arXiv:2105.14103*, 2021.

Yunhao Zhang and Junchi Yan. Crossformer: Transformer utilizing cross-dimension dependency for multivariate time series forecasting. In *The Eleventh International Conference on Learning Representations*, 2023.

Haoyi Zhou, Shanghang Zhang, Jieqi Peng, Shuai Zhang, Jianxin Li, Hui Xiong, and Wancai Zhang. Informer: Beyond efficient transformer for long sequence time-series forecasting. In *Thirty-Fifth AAAI Conference on Artificial Intelligence, AAAI 2021, Thirty-Third Conference on Innovative Applications of Artificial Intelligence, IAAI 2021, The Eleventh Symposium on Educational Advances in Artificial Intelligence, EAAI 2021, Virtual Event, February 2-9, 2021*, pp. 11106–11115. AAAI Press, 2021. URL https://ojs.aaai.org/index.php/AAAI/article/view/17325.

A Appendix

A.1 Datasets

Our main MTSF experiments are conducted on 12 widely-used real-world time series datasets. These datasets are summarized as follows:

Weather Dataset[1] **(Wu et al., 2021)** comprises 21 meteorological variables, including air temperature and humidity, recorded at 10-minute intervals throughout 2020 from the Weather Station of the Max Planck Biogeochemistry Institute in Germany.

Solar Dataset[2] **(Lai et al., 2018)** consists of high-frequency solar power production data from 137 photovoltaic plants recorded throughout 2006. Samples were collected at 10-minute intervals.

Electricity Dataset[3] **(Wu et al., 2021)** contains hourly electricity consumption records for 321 consumers over a three-year period from 2012 to 2014.

ETT Dataset[4] **(Zhou et al., 2021)** The ETT (Electricity Transformer Temperature) Dataset comprises load and oil temperature data from two electricity transformers, recorded at 15-minute and hourly intervals from July 2016 to July 2018. It is divided into four subsets (ETTm1, ETTm2, ETTh1, and ETTh2), each containing seven features related to oil and load characteristics.

Traffic Dataset[5] **(Wu et al., 2021)** Sourced from 862 freeway sensors in the San Francisco Bay area, the Traffic dataset provides hourly road occupancy rates from January 2015 to December 2016. This comprehensive dataset offers consistent measurements across a two-year period.

[1] https://www.bgc-jena.mpg.de/wetter/

[2] http://www.nrel.gov/grid/solar-power-data.html

[3] https://archive.ics.uci.edu/ml/datasets/ElectricityLoadDiagrams20112014

[4] https://github.com/zhouhaoyi/ETDataset

[5] http://pems.dot.ca.gov/

PEMS Dataset[1]**(Li et al., 2017)** The PEMS dataset consists of public traffic network data collected in California at 5-minute intervals. Our study utilizes four widely-adopted subsets (PEMS03, PEMS04, PEMS07, and PEMS08), which have been extensively studied in the field of spatial-temporal time series analysis for traffic prediction tasks.

A.2 Hyper-parameter settings and implementation details

For the hyper-parameter settings of the AR/ARMA Transformer, we use $m = 3$ Transformer layers, 8 heads, and set the hidden dimension d based on the number of series C, using the empirical formula $d = 16\sqrt{C}$. We use $4d$ as the hidden dimension for the feedforward MLP in the Transformer layer. A dropout rate of 0.1 is applied to both the AR term and MA term. We initialize the weights of all linear layers and embedding layers using the GPT-2 weight initialization method, with a normal distribution and a standard deviation of 0.02. For the output projection layers in the attention and MLP, we additionally scale the standard deviation by a factor of $1/\sqrt{m}$, aligned with the GPT-2 setting. Normalization layer is applied both before the input to the Transformer and after the Transformer output. We experimented with both standard LayerNorm and RMSNorm as the normalization layer, finding no significant performance differences, so we opted for RMSNorm for lower computational cost. For token input projection, we use a linear layer to project the L_P-dimensional token to a d-dimensional input vector. In the output projection, we do not tie the weights between the input and output linear layers. A learnable position embedding that maps the integer labels from 1 to N (the input sequence length) to the corresponding d-dimensional position vectors is used. At the beginning of the model, we apply RevIN to input series $\mathbf{S}_I$, subtracting the mean and dividing by the standard deviation for each series. Before outputting the final result, we multiply by the standard deviation and add the mean back. All input series are processed independently and in parallel, merging different series dimensions into the batch size for parallel computation. The random seed used in all the experiments is 2024.

All training tasks in this paper can be conducted using a single Nvidia RTX 4090 GPU. The batch size is set to 32. For larger datasets, such as Traffic and PEMS07, we use a batch size of 16 or 8, with 2-step or 4-step gradient accumulation to ensure the effective batch size for parameter updates remains 32. During training, AR/ARMA Transformers are trained using the next-step prediction objective with MSE loss. We use the AdamW optimizer with betas=(0.9, 0.95) and weight decay=0.1, following the GPT-2 settings. For a fair comparison, the same optimizer is used for training baseline models. It is important to note that the baseline models trained with this AdamW setup show significantly better TSF performance compared to those trained with the default Adam optimizer settings. As a result, the baseline performance presented in this paper may exceed the results reported in their original papers. Since this study focuses on long-term last token prediction results, we apply an additional weight factor to the training loss for the last token, multiplying it by N. However, this weighting only slightly affects performance on smaller datasets with fewer data points, such as ETTs, and has little to no effect on larger datasets. Given the minimal impact of this method, the original next-token MSE loss is sufficient for most datasets, without requiring further modifications.

We use the same train-validation-test set splitting ratio as in previous studies by Zeng et al. (2023); Nie et al. (2022); Liu et al. (2024a). We also follow the same dataset standardization methods used in these studies. During training, we evaluate the validation and test losses at the end of each epoch, with an early-stopping patience set to 12 epochs. The maximum number of training epochs is 100. We apply a linear warm-up for the learning rate, increasing it from 0.00006 to 0.0006 over the first 5 epochs, and gradually decreasing it in the subsequent epochs.

A.3 Supplementary experiment results

In the following section, we provide the complete experimental data corresponding to the tables in the main text. Additionally, we include extra visualizations to help illustrate the actual behavior of the MA weights.

[1] `http://pems.dot.ca.gov/`

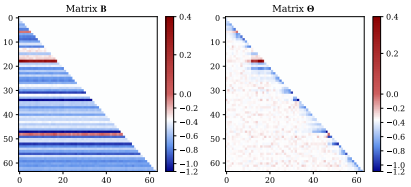

(a) ϕ_q^{MA}: -LeakyReLU, ϕ_k^{MA}: σ ($\alpha = 0.5$)

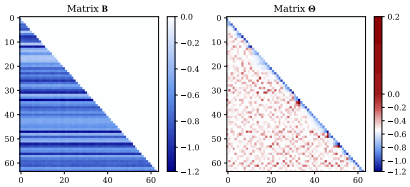

(b) ϕ_q^{MA}: -ReLU, ϕ_k^{MA}: σ ($\alpha = 0.5$)

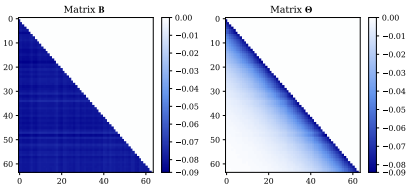

(c) ϕ_q^{MA}: -σ, ϕ_k^{MA}: σ ($\alpha = 0.5$)

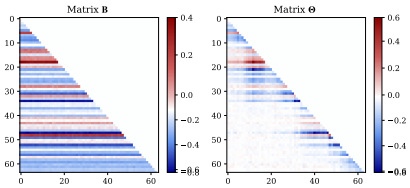

(d) ϕ_q^{MA}: -Swish, ϕ_k^{MA}: σ ($\alpha = 0.5$)

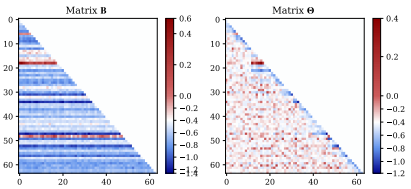

(e) ϕ_q^{MA}: -LeakyReLU, ϕ_k^{MA}: σ ($\alpha = 2$)

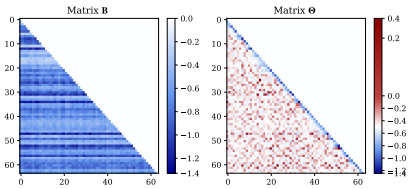

(f) ϕ_q^{MA}: -ReLU, ϕ_k^{MA}: σ ($\alpha = 2$)

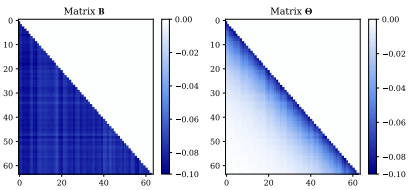

(g) ϕ_q^{MA}: -σ, ϕ_k^{MA}: σ ($\alpha = 2$)

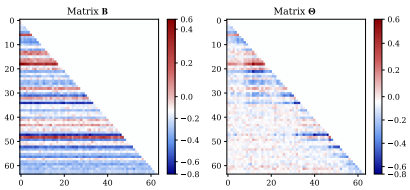

(h) ϕ_q^{MA}: -Swish, ϕ_k^{MA}: σ ($\alpha = 2$)

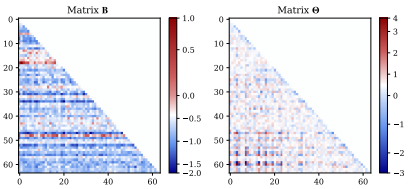

(i) ϕ_q^{MA}: -LeakyReLU, ϕ_k^{MA}: σ ($\alpha = 10$)

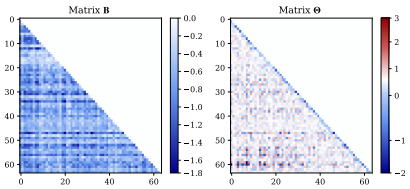

(j) ϕ_q^{MA}: -ReLU, ϕ_k^{MA}: σ ($\alpha = 10$)

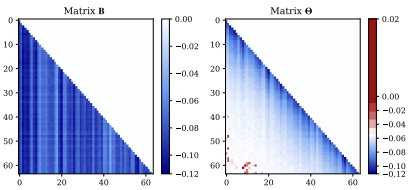

(k) ϕ_q^{MA}: -σ, ϕ_k^{MA}: σ ($\alpha = 10$)

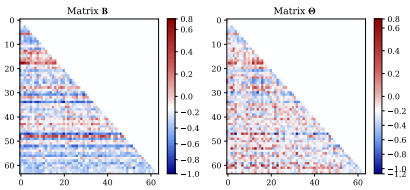

(l) ϕ_q^{MA}: -Swish, ϕ_k^{MA}: σ ($\alpha = 10$)

Figure 7: Additional visualization of $\mathbf{B} - \mathbf{\Theta}$ relationship with different $\phi(\cdot)$ and different α. We construct the simulated $\mathbf{B}$ matrices using randomly sampled $\boldsymbol{q}$ and $\boldsymbol{k}$ ($N = 64$, $d = 32$) from the normal distribution, and display the corresponding $\mathbf{\Theta}$ matrices.

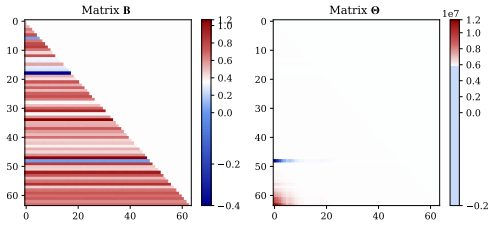

(a) ϕ_q^{MA}: +LeakyReLU, ϕ_k^{MA}: σ ($\alpha = 0.05$)

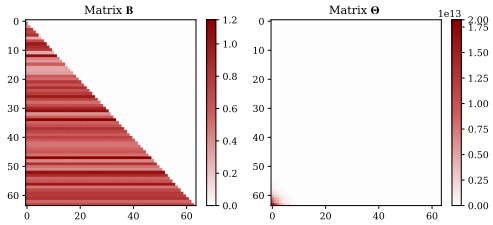

(b) ϕ_q^{MA}: +ReLU, ϕ_k^{MA}: σ ($\alpha = 0.05$)

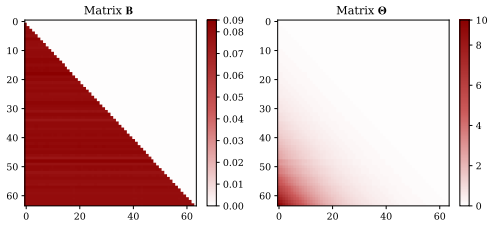

(c) ϕ_q^{MA}: +σ, ϕ_k^{MA}: σ ($\alpha = 0.05$)

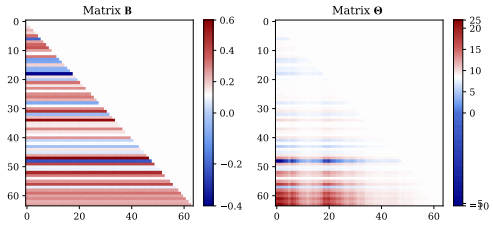

(d) ϕ_q^{MA}: +Swish, ϕ_k^{MA}: σ ($\alpha = 0.05$)

Figure 8: Visualization of $\mathbf{B} - \mathbf{\Theta}$ relationship with positive query activation functions $\phi_q^{\text{MA}}(\cdot)$.

Table 8: Detailed results of main TSF experiments with forecasting horizons $L_P \in \{12, 24, 48, 96\}$ and $L_I = 512$. Test set MSE and MAE for each model on each experiment setup are presented.

Model		Std Attn		Std Attn +ARMA		Lin Attn		Lin Attn +ARMA		GLin Attn		GLin Attn +ARMA		ELin Attn		ELin Attn +ARMA		Fixed Attn		Fixed Attn +ARMA		FITS		iTransformer		CATS		PatchTST		DLinear		EncFormer	
Metrics		MSE	MAE	MSE	MAE	MSE	MAE	MSE	MAE	MSE	MAE	MSE	MAE	MSE	MAE	MSE	MAE	MSE	MAE	MSE	MAE	MSE	MAE	MSE	MAE	MSE	MAE	MSE	MAE	MSE	MAE	MSE	MAE
Weather	96	0.144	0.195	0.142	0.193	0.142	0.194	0.139	0.191	0.161	0.210	0.142	0.194	0.146	0.197	0.143	0.195	0.147	0.194	0.142	0.198	0.151	0.204	0.158	0.140	0.146	0.198	0.149	0.224	0.150	0.209	0.188	0.248
	48	0.113	0.157	0.109	0.151	0.115	0.158	0.110	0.153	0.144	0.191	0.116	0.159	0.114	0.158	0.112	0.156	0.112	0.155	0.115	0.159	0.125	0.177	0.132	0.176	0.116	0.160	0.118	0.161	0.122	0.177	0.143	0.199
	24	0.089	0.118	0.085	0.115	0.088	0.117	0.083	0.114	0.101	0.129	0.090	0.122	0.087	0.116	0.089	0.119	0.091	0.122	0.088	0.120	0.103	0.147	0.101	0.139	0.090	0.125	0.092	0.122	0.147	0.102	0.117	0.162
	12	0.071	0.091	0.067	0.086	0.069	0.088	0.067	0.086	0.070	0.090	0.070	0.091	0.069	0.087	0.069	0.087	0.071	0.089	0.069	0.090	0.078	0.112	0.078	0.105	0.069	0.092	0.070	0.097	0.078	0.115	0.093	0.120
Solar	96	0.196	0.263	0.192	0.257	0.183	0.247	0.180	0.244	0.209	0.283	0.182	0.243	0.194	0.258	0.191	0.257	0.195	0.261	0.187	0.256	0.210	0.254	0.230	0.257	0.182	0.239	0.209	0.251	0.208	0.274	0.201	0.225
	48	0.160	0.230	0.151	0.223	0.152	0.219	0.149	0.217	0.177	0.258	0.154	0.222	0.162	0.236	0.159	0.233	0.161	0.233	0.159	0.229	0.188	0.245	0.189	0.220	0.157	0.209	0.186	0.240	0.184	0.255	0.157	0.186
	24	0.112	0.180	0.098	0.168	0.098	0.166	0.095	0.162	0.143	0.232	0.099	0.167	0.115	0.192	0.113	0.188	0.131	0.221	0.122	0.203	0.132	0.289	0.108	0.163	0.097	0.161	0.129	0.203	0.128	0.208	0.092	0.140
	12	0.069	0.137	0.055	0.118	0.056	0.113	0.052	0.111	0.063	0.139	0.059	0.121	0.072	0.135	0.069	0.133	0.081	0.161	0.070	0.141	0.078	0.159	0.053	0.104	0.052	0.113	0.075	0.155	0.075	0.161	0.048	0.101
ECL	96	0.136	0.233	0.132	0.229	0.130	0.226	0.128	0.225	0.135	0.231	0.133	0.229	0.139	0.237	0.138	0.235	0.142	0.239	0.139	0.236	0.144	0.246	0.132	0.226	0.131	0.229	0.132	0.224	0.135	0.232	0.227	0.342
	48	0.117	0.214	0.113	0.211	0.110	0.207	0.110	0.206	0.113	0.210	0.113	0.210	0.124	0.221	0.121	0.219	0.125	0.223	0.121	0.220	0.129	0.233	0.111	0.207	0.115	0.214	0.112	0.206	0.120	0.219	0.198	0.317
	24	0.097	0.193	0.094	0.190	0.092	0.188	0.091	0.189	0.099	0.197	0.096	0.193	0.103	0.202	0.100	0.199	0.106	0.205	0.104	0.202	0.115	0.221	0.095	0.191	0.101	0.199	0.103	0.196	0.106	0.206	0.183	0.302
	12	0.089	0.188	0.085	0.184	0.091	0.191	0.088	0.189	0.091	0.190	0.088	0.188	0.093	0.197	0.096	0.201	0.110	0.218	0.107	0.215	0.106	0.214	0.084	0.186	0.091	0.192	0.098	0.199	0.096	0.196	0.194	0.313
ETTh1	96	0.357	0.393	0.360	0.395	0.358	0.396	0.361	0.399	0.378	0.406	0.368	0.404	0.360	0.393	0.356	0.393	0.362	0.396	0.359	0.394	0.369	0.398	0.396	0.422	0.371	0.398	0.386	0.407	0.370	0.394	0.986	0.720
	48	0.334	0.375	0.331	0.374	0.331	0.375	0.331	0.376	0.349	0.394	0.337	0.381	0.330	0.372	0.331	0.375	0.331	0.373	0.334	0.378	0.343	0.379	0.362	0.396	0.341	0.379	0.352	0.389	0.342	0.379	0.884	0.670
	24	0.312	0.365	0.299	0.357	0.299	0.356	0.299	0.357	0.349	0.394	0.303	0.360	0.305	0.360	0.305	0.360	0.306	0.361	0.304	0.360	0.318	0.366	0.334	0.381	0.313	0.365	0.313	0.361	0.312	0.362	0.792	0.676
	12	0.290	0.345	0.280	0.340	0.285	0.342	0.272	0.337	0.554	0.503	0.277	0.340	0.296	0.351	0.293	0.348	0.320	0.374	0.316	0.368	0.301	0.357	0.310	0.363	0.281	0.341	0.290	0.345	0.291	0.348	0.607	0.534
ETTh2	96	0.266	0.330	0.268	0.331	0.273	0.336	0.275	0.338	0.285	0.338	0.281	0.345	0.267	0.333	0.263	0.329	0.288	0.345	0.276	0.337	0.270	0.336	0.373	0.394	0.270	0.338	0.274	0.341	0.277	0.346	1.303	0.924
	48	0.213	0.290	0.216	0.294	0.215	0.290	0.217	0.293	0.233	0.294	0.220	0.295	0.212	0.290	0.210	0.288	0.215	0.290	0.208	0.288	0.217	0.298	0.226	0.310	0.212	0.299	0.222	0.304	0.217	0.301	0.568	0.596
	24	0.160	0.252	0.160	0.252	0.159	0.250	0.162	0.252	0.182	0.263	0.164	0.254	0.162	0.249	0.158	0.249	0.158	0.250	0.158	0.251	0.168	0.264	0.178	0.275	0.167	0.262	0.174	0.269	0.166	0.263	0.290	0.405
	12	0.129	0.229	0.125	0.224	0.124	0.224	0.125	0.224	0.168	0.263	0.127	0.224	0.129	0.228	0.128	0.230	0.139	0.240	0.133	0.235	0.133	0.239	0.139	0.248	0.128	0.235	0.135	0.242	0.131	0.237	0.225	0.354
ETTm1	96	0.305	0.359	0.301	0.354	0.303	0.355	0.296	0.351	0.336	0.382	0.299	0.355	0.305	0.356	0.301	0.354	0.298	0.347	0.296	0.344	0.305	0.347	0.352	0.378	0.300	0.354	0.323	0.362	0.305	0.348	0.686	0.603
	48	0.287	0.344	0.276	0.333	0.278	0.336	0.266	0.328	0.500	0.472	0.372	0.334	0.284	0.346	0.282	0.342	0.284	0.338	0.280	0.340	0.280	0.331	0.304	0.346	0.266	0.328	0.289	0.341	0.278	0.329	0.475	0.474
	24	0.246	0.312	0.223	0.293	0.218	0.293	0.196	0.279	0.473	0.429	0.225	0.305	0.239	0.305	0.241	0.307	0.284	0.332	0.255	0.321	0.218	0.289	0.223	0.293	0.197	0.277	0.235	0.304	0.216	0.288	0.352	0.391
	12	0.218	0.287	0.156	0.241	0.151	0.240	0.128	0.222	0.320	0.335	0.144	0.237	0.157	0.247	0.153	0.246	0.203	0.282	0.174	0.261	0.144	0.235	0.155	0.246	0.125	0.222	0.128	0.224	0.140	0.230	0.204	0.294
ETTm2	96	0.177	0.262	0.174	0.261	0.167	0.255	0.162	0.250	0.178	0.260	0.172	0.258	0.178	0.260	0.174	0.260	0.167	0.254	0.166	0.254	0.164	0.253	0.198	0.277	0.168	0.255	0.177	0.266	0.184	0.283	0.481	0.525
	48	0.139	0.238	0.137	0.236	0.145	0.248	0.143	0.250	0.167	0.264	0.148	0.249	0.153	0.253	0.139	0.238	0.146	0.245	0.138	0.238	0.126	0.225	0.147	0.242	0.127	0.227	0.131	0.231	0.125	0.226	0.483	0.516
	24	0.121	0.219	0.117	0.217	0.110	0.211	0.101	0.199	0.132	0.227	0.110	0.209	0.117	0.217	0.116	0.216	0.119	0.220	0.119	0.221	0.096	0.195	0.112	0.212	0.096	0.195	0.097	0.194	0.095	0.194	0.162	0.280
	12	0.086	0.175	0.083	0.174	0.083	0.174	0.078	0.169	0.089	0.178	0.082	0.172	0.086	0.174	0.083	0.174	0.085	0.177	0.083	0.174	0.073	0.168	0.082	0.181	0.072	0.165	0.072	0.165	0.077	0.195	0.116	0.231
Traffic	96	0.379	0.273	0.373	0.269	0.365	0.262	0.362	0.260	0.474	0.324	0.381	0.275	0.381	0.270	0.378	0.271	0.393	0.279	0.389	0.277	0.404	0.286	0.356	0.259	0.377	0.284	0.381	0.298	0.399	0.286	0.915	0.460
	48	0.352	0.256	0.342	0.253	0.349	0.251	0.339	0.254	0.569	0.371	0.375	0.271	0.363	0.263	0.359	0.261	0.374	0.275	0.365	0.265	0.393	0.286	0.341	0.264	0.369	0.271	0.373	0.275	0.385	0.284	0.857	0.434
	24	0.324	0.238	0.315	0.231	0.322	0.239	0.318	0.238	0.346	0.257	0.330	0.245	0.334	0.247	0.330	0.243	0.344	0.256	0.340	0.251	0.374	0.280	0.318	0.250	0.372	0.279	0.345	0.262	0.363	0.271	0.814	0.417
	12	0.310	0.230	0.303	0.228	0.311	0.232	0.302	0.227	0.325	0.250	0.313	0.236	0.330	0.255	0.326	0.252	0.379	0.285	0.364	0.281	0.370	0.282	0.303	0.238	0.369	0.268	0.331	0.253	0.353	0.270	0.801	0.403
PEM503	96	0.171	0.280	0.153	0.263	0.149	0.258	0.143	0.252	0.360	0.416	0.147	0.257	0.173	0.281	0.169	0.279	0.178	0.285	0.174	0.280	0.193	0.274	0.135	0.229	0.157	0.267	0.198	0.285	0.198	0.299	0.162	0.272
	48	0.122	0.234	0.106	0.217	0.105	0.215	0.102	0.210	0.299	0.380	0.109	0.216	0.128	0.235	0.123	0.248	0.131	0.243	0.126	0.237	0.155	0.247	0.108	0.215	0.116	0.230	0.167	0.266	0.155	0.260	0.117	0.234
	24	0.089	0.201	0.079	0.187	0.081	0.188	0.075	0.181	0.097	0.209	0.082	0.189	0.091	0.199	0.089	0.201	0.099	0.213	0.095	0.209	0.108	0.211	0.078	0.184	0.085	0.196	0.108	0.221	0.109	0.218	0.089	0.201
	12	0.067	0.173	0.063	0.167	0.065	0.169	0.062	0.165	0.078	0.185	0.067	0.177	0.071	0.178	0.068	0.176	0.077	0.187	0.070	0.176	0.076	0.180	0.062	0.166	0.061	0.166	0.088	0.209	0.075	0.184	0.075	0.186
PEM504	96	0.154	0.265	0.139	0.250	0.133	0.240	0.131	0.237	0.166	0.277	0.135	0.243	0.163	0.275	0.158	0.270	0.171	0.284	0.168	0.280	0.215	0.299	0.121	0.217	0.141	0.253	0.221	0.320	0.209	0.301	0.116	0.232
	48	0.133	0.246	0.119	0.230	0.114	0.223	0.106	0.217	0.299	0.389	0.113	0.225	0.138	0.251	0.135	0.247	0.153	0.253	0.135	0.250	0.173	0.270	0.109	0.205	0.126	0.247	0.214	0.340	0.167	0.268	0.103	0.216
	24	0.103	0.215	0.092	0.199	0.091	0.199	0.085	0.194	0.116	0.230	0.094	0.202	0.103	0.217	0.103	0.215	0.113	0.227	0.107	0.218	0.124	0.230	0.087	0.186	0.090	0.201	0.131	0.243	0.123	0.229	0.092	0.203
	12	0.082	0.190	0.075	0.179	0.075	0.180	0.070	0.176	0.087	0.195	0.078	0.183	0.085	0.191	0.081	0.188	0.089	0.198	0.085	0.193	0.092	0.199	0.073	0.174	0.074	0.180	0.089	0.196	0.091	0.197	0.085	0.193
PEM507	96	0.126	0.237	0.118	0.227	0.113	0.220	0.117	0.225	0.126	0.137	0.118	0.228	0.138	0.248	0.133	0.245	0.141	0.256	0.139	0.251	0.193	0.289	0.119	0.210	0.144	0.257	0.132	0.245	0.178	0.278	0.145	0.258
	48	0.091	0.201	0.082	0.189	0.084	0.185	0.071	0.179	0.093	0.204	0.085	0.199	0.109	0.222	0.106	0.219	0.114	0.227	0.109	0.224	0.152	0.254	0.072	0.171	0.102	0.212	0.091	0.206	0.155	0.257	0.104	0.216
	24	0.080	0.189	0.068	0.171	0.079	0.189	0.065	0.169	0.080	0.188	0.077	0.186	0.086	0.199	0.081	0.190	0.094	0.206	0.086	0.196	0.106	0.213	0.068	0.156	0.075	0.181	0.082	0.193	0.107	0.218	0.086	0.196
	12	0.072	0.180	0.063	0.168	0.072	0.189	0.055	0.152	0.072	0.184	0.068	0.180	0.071	0.181	0.069	0.178	0.073	0.184	0.067	0.174	0.075	0.178	0.055	0.150	0.056	0.154	0.066	0.162	0.074	0.179	0.073	0.180
PEM508	96	0.222	0.262	0.207	0.249	0.179	0.235	0.175	0.233	0.255	0.291	0.194	0.238	0.229	0.271	0.221	0.268	0.234	0.273	0.226	0.269	0.337	0.322	0.170	0.215	0.212	0.276	0.183	0.236	0.318	0.326	0.253	0.302
	48	0.166	0.241	0.141	0.222	0.128	0.215	0.125	0.208	0.191	0.269	0.138	0.228	0.172	0.248	0.164	0.247	0.188	0.263	0.164	0.248	0.232	0.282	0.131	0.197	0.142	0.238	0.136	0.225	0.223	0.283	0.203	0.279
	24	0.114	0.209	0.102	0.192	0.095	0.191	0.086	0.184	0.112	0.212	0.098	0.199	0.112	0.213	0.109	0.211	0.118	0.221	0.114	0.214	0.142	0.233	0.090	0.183	0.107	0.203	0.091	0.199	0.137	0.232	0.154	0.238
	12	0.088	0.189	0.077	0.173	0.074	0.171	0.076	0.175	0.079	0.182	0.071	0.170	0.086	0.185	0.082	0.186	0.103	0.225	0.105	0.221	0.094	0.196	0.076	0.171	0.078	0.177	0.073	0.176	0.092	0.195	0.123	0.216

Table 9: Results showing that ARMA Transformers with $m = 3$ layers consistently outperform their AR counterparts across a wide range of m. Forecasting horizons $L_P \in \{12, 24, 48, 96\}$ and $L_I = 512$ are used. Test set MSE and MAE for each model on each experiment setup are presented.

		Model	ARMA(m=3)		AR(m=1)		AR(m=2)		AR(m=3)		AR(m=4)		AR(m=5)		AR(m=6)		AR(m=7)		AR(m=8)	
		Metrics	MSE	MAE	MSE	MAE	MSE	MAE	MSE	MAE	MSE	MAE	MSE	MAE	MSE	MAE	MSE	MAE	MSE	MAE
ETTm1	96	Std Attn	0.301	0.354	0.305	0.360	0.308	0.360	0.305	0.359	0.308	0.360	0.304	0.358	0.309	0.361	0.306	0.359	0.307	0.359
		Lin Attn	0.296	0.351	0.310	0.361	0.301	0.358	0.303	0.355	0.303	0.356	0.299	0.352	0.301	0.355	0.299	0.353	0.300	0.354
		GLin Attn	0.299	0.355	0.337	0.381	0.337	0.387	0.336	0.382	0.334	0.380	0.337	0.382	0.337	0.382	0.335	0.381	0.333	0.379
		ELin Attn	0.301	0.354	0.307	0.363	0.309	0.361	0.305	0.356	0.307	0.360	0.306	0.359	0.309	0.362	0.305	0.359	0.308	0.361
		Fixed Attn	0.296	0.344	0.299	0.346	0.298	0.349	0.298	0.347	0.299	0.347	0.300	0.348	0.298	0.347	0.302	0.348	0.305	0.351
	48	Std Attn	0.276	0.333	0.293	0.347	0.293	0.347	0.287	0.344	0.290	0.345	0.290	0.345	0.288	0.344	0.286	0.342	0.291	0.345
		Lin Attn	0.266	0.328	0.280	0.336	0.278	0.337	0.278	0.336	0.278	0.336	0.271	0.331	0.272	0.333	0.274	0.332	0.276	0.334
		GLin Attn	0.372	0.334	0.494	0.347	0.496	0.464	0.500	0.472	0.505	0.467	0.500	0.468	0.516	0.459	0.494	0.469	0.499	0.469
		ELin Attn	0.282	0.342	0.293	0.350	0.289	0.350	0.284	0.346	0.292	0.349	0.294	0.352	0.295	0.352	0.292	0.350	0.299	0.355
		Fixed Attn	0.280	0.340	0.286	0.345	0.283	0.340	0.284	0.338	0.283	0.340	0.284	0.338	0.277	0.335	0.282	0.335	0.279	0.336
	24	Std Attn	0.223	0.293	0.234	0.300	0.258	0.323	0.246	0.312	0.244	0.311	0.262	0.325	0.260	0.324	0.259	0.323	0.263	0.327
		Lin Attn	0.196	0.279	0.226	0.297	0.210	0.288	0.218	0.293	0.211	0.288	0.210	0.286	0.208	0.285	0.212	0.287	0.209	0.287
		GLin Attn	0.225	0.305	0.487	0.430	0.499	0.440	0.473	0.429	0.476	0.436	0.482	0.436	0.466	0.435	0.486	0.440	0.463	0.430
		ELin Attn	0.241	0.307	0.253	0.328	0.246	0.317	0.239	0.305	0.253	0.318	0.268	0.327	0.263	0.322	0.264	0.325	0.264	0.326
		Fixed Attn	0.255	0.321	0.274	0.317	0.272	0.334	0.284	0.332	0.260	0.326	0.254	0.320	0.266	0.329	0.257	0.322	0.255	0.322
	12	Std Attn	0.156	0.241	0.229	0.293	0.222	0.288	0.218	0.287	0.221	0.291	0.221	0.289	0.223	0.291	0.228	0.288	0.227	0.287
		Lin Attn	0.128	0.222	0.148	0.239	0.141	0.232	0.151	0.240	0.137	0.228	0.138	0.234	0.139	0.231	0.137	0.228	0.138	0.229
		GLin Attn	0.144	0.237	0.325	0.325	0.321	0.324	0.320	0.335	0.319	0.326	0.322	0.326	0.322	0.325	0.320	0.323	0.320	0.323
		ELin Attn	0.153	0.246	0.160	0.251	0.160	0.252	0.157	0.247	0.159	0.250	0.160	0.252	0.169	0.260	0.163	0.251	0.160	0.247
		Fixed Attn	0.174	0.261	0.215	0.289	0.204	0.285	0.203	0.282	0.199	0.281	0.194	0.279	0.195	0.278	0.192	0.275	0.189	0.278
Weather	96	Std Attn	0.142	0.193	0.156	0.207	0.153	0.210	0.144	0.195	0.152	0.206	0.156	0.201	0.156	0.209	0.156	0.207	0.156	0.207
		Lin Attn	0.139	0.191	0.144	0.197	0.143	0.195	0.142	0.194	0.143	0.196	0.143	0.194	0.143	0.194	0.142	0.193	0.144	0.196
		GLin Attn	0.142	0.194	0.163	0.213	0.163	0.212	0.161	0.210	0.165	0.213	0.163	0.212	0.164	0.213	0.164	0.216	0.164	0.213
		ELin Attn	0.143	0.195	0.157	0.211	0.148	0.207	0.146	0.197	0.151	0.211	0.156	0.208	0.157	0.211	0.156	0.207	0.157	0.208
		Fixed Attn	0.142	0.198	0.158	0.210	0.151	0.209	0.147	0.194	0.152	0.206	0.154	0.206	0.153	0.204	0.153	0.207	0.153	0.205
	48	Std Attn	0.109	0.151	0.116	0.161	0.115	0.159	0.113	0.157	0.116	0.160	0.127	0.177	0.120	0.168	0.128	0.181	0.127	0.177
		Lin Attn	0.110	0.153	0.114	0.156	0.113	0.156	0.115	0.158	0.113	0.153	0.113	0.155	0.112	0.153	0.112	0.155	0.112	0.155
		GLin Attn	0.116	0.159	0.144	0.190	0.144	0.189	0.144	0.191	0.145	0.193	0.145	0.191	0.144	0.192	0.143	0.189	0.143	0.189
		ELin Attn	0.112	0.156	0.119	0.167	0.116	0.166	0.114	0.158	0.117	0.166	0.118	0.165	0.122	0.172	0.121	0.167	0.123	0.171
		Fixed Attn	0.115	0.159	0.124	0.171	0.118	0.170	0.112	0.155	0.122	0.170	0.126	0.173	0.121	0.171	0.122	0.168	0.121	0.167
	24	Std Attn	0.085	0.115	0.091	0.124	0.091	0.124	0.089	0.118	0.093	0.124	0.096	0.132	0.095	0.130	0.095	0.129	0.094	0.126
		Lin Attn	0.083	0.114	0.087	0.117	0.087	0.118	0.088	0.117	0.087	0.115	0.086	0.116	0.087	0.118	0.087	0.117	0.087	0.116
		GLin Attn	0.090	0.122	0.103	0.132	0.103	0.132	0.101	0.129	0.103	0.132	0.103	0.129	0.103	0.134	0.104	0.132	0.103	0.132
		ELin Attn	0.089	0.119	0.092	0.123	0.092	0.123	0.087	0.116	0.090	0.122	0.092	0.128	0.092	0.128	0.092	0.127	0.092	0.124
		Fixed Attn	0.088	0.120	0.095	0.127	0.093	0.126	0.091	0.122	0.094	0.128	0.094	0.125	0.093	0.125	0.092	0.124	0.094	0.127
	12	Std Attn	0.067	0.086	0.073	0.091	0.072	0.091	0.071	0.091	0.072	0.093	0.072	0.091	0.072	0.091	0.072	0.094	0.072	0.091
		Lin Attn	0.067	0.086	0.069	0.088	0.069	0.089	0.069	0.088	0.069	0.089	0.068	0.088	0.068	0.087	0.068	0.088	0.069	0.090
		GLin Attn	0.070	0.091	0.078	0.092	0.077	0.095	0.070	0.090	0.072	0.093	0.071	0.088	0.077	0.093	0.071	0.088	0.071	0.090
		ELin Attn	0.069	0.087	0.071	0.090	0.071	0.091	0.069	0.087	0.072	0.091	0.071	0.091	0.071	0.090	0.072	0.091	0.071	0.090
		Fixed Attn	0.069	0.090	0.073	0.093	0.072	0.094	0.071	0.089	0.072	0.093	0.072	0.091	0.072	0.090	0.072	0.089	0.072	0.091

Table 10: Results showing that AR/ARMA Transformers effectively utilize extended lookback L_I, while baselines experience performance degradation. $L_I \in \{512, 1024, 2048, 4096\}$ with $L_P \in \{12, 24, 48, 96\}$ are evaluated. Test set MSE and MAE for each model on each setup are presented.

Model			Std Attn		Std Attn +ARMA		Lin Attn		Lin Attn +ARMA		GLin Attn		GLin Attn +ARMA		ELin Attn		ELin Attn +ARMA		Fixed Attn		Fixed Attn +ARMA		FITS		iTransformer		CATS		PatchTST		DLinear		EncFormer	
Metrics			MSE	MAE	MSE	MAE	MSE	MAE	MSE	MAE	MSE	MAE	MSE	MAE	MSE	MAE	MSE	MAE	MSE	MAE	MSE	MAE	MSE	MAE	MSE	MAE	MSE	MAE	MSE	MAE	MSE	MAE	MSE	MAE
Weather	512	96	0.144	0.195	0.142	0.193	0.142	0.194	0.139	0.191	0.161	0.210	0.142	0.194	0.145	0.197	0.143	0.195	0.147	0.194	0.142	0.198	0.151	0.204	0.158	0.140	0.146	0.198	0.151	0.224	0.150	0.209	0.188	0.248
		48	0.113	0.157	0.109	0.151	0.115	0.158	0.110	0.153	0.144	0.191	0.116	0.159	0.114	0.158	0.112	0.156	0.112	0.155	0.115	0.159	0.125	0.177	0.132	0.176	0.116	0.160	0.118	0.161	0.122	0.177	0.143	0.199
		24	0.089	0.118	0.085	0.115	0.088	0.117	0.083	0.114	0.101	0.129	0.090	0.122	0.087	0.116	0.089	0.119	0.091	0.122	0.088	0.120	0.103	0.147	0.101	0.139	0.090	0.125	0.092	0.122	0.147	0.102	0.117	0.162
		12	0.071	0.091	0.067	0.086	0.069	0.088	0.067	0.086	0.070	0.090	0.070	0.091	0.069	0.087	0.069	0.087	0.071	0.089	0.069	0.090	0.078	0.112	0.078	0.105	0.069	0.092	0.071	0.097	0.078	0.115	0.093	0.120
	1024	96	0.145	0.196	0.142	0.194	0.144	0.198	0.141	0.195	0.161	0.212	0.145	0.198	0.147	0.198	0.144	0.197	0.149	0.201	0.144	0.198	0.168	0.222	0.164	0.219	0.148	0.203	0.167	0.223	0.166	0.222	0.175	0.247
		48	0.112	0.156	0.110	0.152	0.110	0.154	0.109	0.152	0.144	0.193	0.115	0.157	0.114	0.159	0.117	0.156	0.116	0.161	0.114	0.162	0.132	0.185	0.127	0.181	0.118	0.164	0.133	0.187	0.129	0.181	0.141	0.202
		24	0.096	0.130	0.088	0.118	0.086	0.112	0.086	0.116	0.091	0.123	0.089	0.122	0.090	0.122	0.091	0.123	0.095	0.129	0.092	0.126	0.102	0.147	0.098	0.141	0.091	0.128	0.101	0.144	0.100	0.144	0.104	0.146
		12	0.075	0.092	0.068	0.086	0.068	0.088	0.067	0.087	0.069	0.090	0.068	0.087	0.073	0.092	0.071	0.090	0.072	0.092	0.071	0.091	0.078	0.112	0.078	0.114	0.073	0.102	0.077	0.110	0.077	0.112	0.075	0.119
	2048	96	0.154	0.208	0.144	0.200	0.139	0.195	0.139	0.195	0.145	0.216	0.144	0.200	0.155	0.210	0.153	0.209	0.155	0.213	0.152	0.216	0.169	0.225	0.164	0.220	0.154	0.212	0.168	0.224	0.167	0.223	0.194	0.270
		48	0.114	0.159	0.110	0.157	0.110	0.155	0.108	0.152	0.146	0.198	0.110	0.155	0.115	0.163	0.115	0.163	0.132	0.184	0.123	0.173	0.134	0.187	0.128	0.184	0.122	0.176	0.135	0.190	0.131	0.185	0.129	0.190
		24	0.097	0.135	0.085	0.119	0.086	0.115	0.085	0.117	0.096	0.122	0.087	0.118	0.090	0.125	0.090	0.125	0.132	0.096	0.093	0.128	0.102	0.149	0.101	0.150	0.096	0.135	0.103	0.152	0.100	0.146	0.108	0.157
		12	0.073	0.094	0.068	0.089	0.068	0.088	0.067	0.086	0.069	0.090	0.068	0.089	0.072	0.093	0.072	0.093	0.073	0.095	0.072	0.093	0.080	0.120	0.082	0.127	0.078	0.104	0.080	0.124	0.077	0.117	0.079	0.111
	4096	96	0.150	0.207	0.143	0.203	0.139	0.198	0.139	0.201	0.166	0.220	0.142	0.201	0.153	0.213	0.150	0.212	0.157	0.215	0.155	0.213	0.168	0.228	0.168	0.231	0.164	0.225	0.171	0.232	0.171	0.235	0.212	0.281
		48	0.114	0.162	0.111	0.159	0.109	0.155	0.107	0.156	0.137	0.193	0.123	0.176	0.117	0.168	0.116	0.166	0.117	0.168	0.111	0.159	0.135	0.194	0.173	0.201	0.138	0.194	0.138	0.199	0.132	0.191	0.139	0.194
		24	0.097	0.140	0.085	0.122	0.085	0.117	0.085	0.118	0.086	0.121	0.086	0.120	0.093	0.130	0.089	0.125	0.096	0.132	0.094	0.129	0.105	0.156	0.103	0.154	0.108	0.153	0.107	0.162	0.102	0.152	0.114	0.160
		12	0.072	0.096	0.067	0.089	0.068	0.088	0.068	0.088	0.070	0.092	0.068	0.089	0.071	0.096	0.071	0.097	0.071	0.097	0.071	0.096	0.086	0.135	0.085	0.133	0.081	0.118	0.085	0.140	0.079	0.112	0.080	0.110
ETTm1	512	96	0.305	0.359	0.301	0.354	0.303	0.355	0.296	0.351	0.336	0.382	0.299	0.355	0.305	0.356	0.301	0.354	0.298	0.347	0.296	0.344	0.305	0.347	0.352	0.378	0.300	0.354	0.323	0.362	0.305	0.348	0.686	0.603
		48	0.287	0.344	0.276	0.333	0.278	0.336	0.266	0.328	0.500	0.472	0.372	0.334	0.284	0.342	0.284	0.338	0.284	0.342	0.280	0.340	0.280	0.331	0.304	0.346	0.266	0.328	0.289	0.341	0.278	0.329	0.475	0.474
		24	0.246	0.312	0.223	0.293	0.218	0.293	0.196	0.279	0.473	0.429	0.225	0.305	0.239	0.305	0.241	0.307	0.284	0.332	0.255	0.321	0.218	0.289	0.223	0.293	0.197	0.277	0.235	0.304	0.216	0.288	0.352	0.391
		12	0.218	0.287	0.156	0.241	0.151	0.240	0.128	0.222	0.320	0.335	0.144	0.237	0.157	0.247	0.153	0.246	0.203	0.282	0.174	0.261	0.144	0.235	0.155	0.246	0.125	0.222	0.128	0.224	0.140	0.230	0.204	0.294
	1024	96	0.318	0.366	0.308	0.357	0.305	0.356	0.304	0.357	0.339	0.384	0.309	0.362	0.317	0.367	0.308	0.359	0.306	0.356	0.303	0.353	0.310	0.353	0.340	0.377	0.314	0.367	0.321	0.363	0.308	0.353	0.493	0.497
		48	0.308	0.355	0.281	0.333	0.292	0.345	0.272	0.333	0.532	0.486	0.277	0.340	0.315	0.363	0.296	0.349	0.303	0.356	0.300	0.351	0.285	0.337	0.310	0.350	0.293	0.346	0.290	0.340	0.287	0.344	0.442	0.423
		24	0.267	0.332	0.231	0.305	0.221	0.294	0.202	0.282	0.504	0.441	0.218	0.298	0.266	0.328	0.252	0.316	0.292	0.352	0.271	0.330	0.222	0.293	0.228	0.301	0.210	0.289	0.219	0.292	0.219	0.292	0.338	0.373
		12	0.228	0.236	0.145	0.299	0.138	0.229	0.130	0.222	0.317	0.323	0.140	0.232	0.160	0.248	0.157	0.251	0.221	0.292	0.179	0.269	0.144	0.237	0.153	0.249	0.133	0.229	0.151	0.245	0.140	0.232	0.182	0.268
	2048	96	0.314	0.364	0.302	0.357	0.301	0.356	0.301	0.356	0.342	0.387	0.304	0.360	0.313	0.366	0.305	0.360	0.304	0.358	0.304	0.356	0.311	0.356	0.330	0.373	0.335	0.384	0.318	0.366	0.311	0.360	0.503	0.504
		48	0.302	0.353	0.281	0.334	0.282	0.339	0.266	0.331	0.529	0.482	0.272	0.338	0.309	0.364	0.298	0.355	0.312	0.369	0.314	0.369	0.287	0.341	0.290	0.341	0.307	0.359	0.305	0.361	0.281	0.339	0.529	0.563
		24	0.270	0.337	0.228	0.305	0.214	0.290	0.198	0.283	0.272	0.330	0.211	0.293	0.273	0.330	0.244	0.314	0.312	0.367	0.279	0.338	0.221	0.298	0.225	0.304	0.253	0.324	0.217	0.294	0.220	0.298	0.409	0.436
		12	0.226	0.238	0.146	0.296	0.136	0.232	0.128	0.222	0.164	0.255	0.140	0.238	0.229	0.295	0.162	0.252	0.225	0.294	0.173	0.260	0.163	0.258	0.147	0.201	0.148	0.251	0.160	0.257	0.142	0.239	0.218	0.306
	4096	96	0.305	0.365	0.296	0.356	0.299	0.361	0.298	0.359	0.338	0.385	0.296	0.356	0.306	0.366	0.298	0.359	0.303	0.362	0.299	0.356	0.319	0.366	0.357	0.394	0.454	0.455	0.317	0.364	0.324	0.368	0.619	0.576
		48	0.298	0.354	0.276	0.339	0.292	0.350	0.274	0.342	0.551	0.502	0.272	0.341	0.318	0.374	0.293	0.357	0.332	0.386	0.316	0.370	0.299	0.353	0.315	0.365	0.387	0.415	0.321	0.373	0.296	0.354	0.481	0.509
		24	0.266	0.331	0.227	0.302	0.220	0.303	0.203	0.291	0.252	0.322	0.211	0.298	0.269	0.333	0.252	0.325	0.343	0.386	0.279	0.344	0.231	0.308	0.245	0.323	0.306	0.351	0.225	0.300	0.230	0.309	0.368	0.406
		12	0.230	0.298	0.138	0.233	0.135	0.231	0.129	0.224	0.156	0.246	0.137	0.232	0.233	0.299	0.217	0.292	0.170	0.298	0.168	0.260	0.160	0.260	0.178	0.274	0.213	0.307	0.176	0.278	0.148	0.251	0.243	0.339

Table 11: Results of model performance on varying horizons L_P. AR/ARMA Transformers uses $L_I = 512$ for $L_P = 1$ and $L_I = 4096$ for $L_P = 720$. Baselines are consistently set to their best-performing $L_I = 512$ configuration. Test set MSE and MAE for each model on each setup are reported.

Model		Std Attn		Std Attn +ARMA		Lin Attn		Lin Attn +ARMA		GLin Attn		GLin Attn +ARMA		ELin Attn		ELin Attn +ARMA		Fixed Attn		Fixed Attn +ARMA		FITS		iTransformer		CATS		PatchTST		DLinear		EncFormer	
Metrics		MSE	MAE	MSE	MAE	MSE	MAE	MSE	MAE	MSE	MAE	MSE	MAE	MSE	MAE	MSE	MAE	MSE	MAE	MSE	MAE	MSE	MAE	MSE	MAE	MSE	MAE	MSE	MAE	MSE	MAE	MSE	MAE
ETTm1	1	0.048	0.140	0.043	0.130	0.042	0.126	0.041	0.123	0.051	0.138	0.043	0.126	0.053	0.140	0.051	0.140	0.054	0.142	0.052	0.140	0.047	0.138	0.049	0.151	0.043	0.127	0.046	0.133	0.044	0.130	0.044	0.129
	720	0.396	0.418	0.391	0.416	0.417	0.435	0.408	0.429	0.396	0.419	0.393	0.418	0.395	0.419	0.391	0.416	0.403	0.423	0.399	0.421	0.420	0.412	0.438	0.440	0.418	0.415	0.408	0.422	0.420	0.416	0.802	0.676
ETTm2	1	0.034	0.096	0.030	0.095	0.032	0.094	0.029	0.092	0.033	0.093	0.030	0.092	0.035	0.095	0.033	0.093	0.033	0.095	0.031	0.093	0.034	0.108	0.034	0.112	0.032	0.079	0.033	0.102	0.031	0.098	0.035	0.118
	720	0.329	0.373	0.327	0.371	0.341	0.383	0.338	0.381	0.334	0.373	0.328	0.374	0.327	0.372	0.326	0.371	0.331	0.378	0.327	0.373	0.360	0.381	0.369	0.391	0.351	0.379	0.362	0.383	0.403	0.426	2.641	1.387
Weather	1	0.037	0.046	0.032	0.044	0.032	0.042	0.031	0.041	0.033	0.044	0.031	0.041	0.037	0.049	0.034	0.047	0.036	0.045	0.034	0.044	0.038	0.059	0.038	0.064	0.033	0.046	0.035	0.054	0.034	0.052	0.032	0.046
	720	0.299	0.328	0.301	0.332	0.308	0.336	0.305	0.337	0.310	0.334	0.299	0.332	0.296	0.326	0.295	0.325	0.299	0.327	0.297	0.326	0.327	0.342	0.317	0.335	0.311	0.334	0.325	0.340	0.319	0.356	0.404	0.423

Table 12: Experiment results of the performance comparison with MEGA with $L_P \in \{12, 24, 48, 96\}$.

Model		Std Attn		Std Attn +ARMA		Lin Attn		Lin Attn +ARMA		GLin Attn		GLin Attn +ARMA		MEGA	
Metrics		MSE	MAE	MSE	MAE	MSE	MAE	MSE	MAE	MSE	MAE	MSE	MAE	MSE	MAE
Weather	96	0.144	0.195	0.142	0.193	0.142	0.194	0.139	0.191	0.161	0.210	0.142	0.194	0.164	0.212
	48	0.113	0.157	0.109	0.151	0.115	0.158	0.110	0.153	0.144	0.191	0.116	0.159	0.141	0.187
	24	0.089	0.118	0.085	0.115	0.088	0.117	0.083	0.114	0.101	0.129	0.090	0.122	0.102	0.128
	12	0.071	0.091	0.067	0.086	0.069	0.088	0.067	0.086	0.070	0.090	0.070	0.091	0.077	0.090
Solar	96	0.196	0.263	0.192	0.257	0.183	0.247	0.180	0.244	0.209	0.283	0.182	0.243	0.235	0.302
	48	0.160	0.230	0.151	0.223	0.152	0.219	0.149	0.217	0.177	0.258	0.154	0.222	0.342	0.406
	24	0.112	0.180	0.098	0.168	0.098	0.166	0.095	0.162	0.143	0.232	0.099	0.167	0.231	0.284
	12	0.069	0.137	0.055	0.118	0.056	0.113	0.052	0.111	0.063	0.139	0.059	0.121	0.097	0.170
ETTh1	96	0.357	0.393	0.360	0.395	0.358	0.396	0.361	0.399	0.378	0.406	0.368	0.404	0.373	0.468
	48	0.334	0.375	0.331	0.374	0.331	0.375	0.331	0.376	0.349	0.386	0.337	0.381	0.348	0.386
	24	0.312	0.365	0.299	0.357	0.299	0.356	0.299	0.357	0.349	0.394	0.303	0.360	0.345	0.387
	12	0.290	0.345	0.280	0.340	0.285	0.342	0.272	0.337	0.554	0.503	0.277	0.340	0.551	0.499
ETTh2	96	0.266	0.330	0.268	0.331	0.273	0.336	0.275	0.338	0.285	0.338	0.281	0.345	0.278	0.330
	48	0.213	0.290	0.216	0.294	0.215	0.290	0.217	0.293	0.233	0.294	0.220	0.295	0.230	0.295
	24	0.160	0.252	0.160	0.252	0.159	0.250	0.162	0.252	0.182	0.263	0.164	0.254	0.180	0.261
	12	0.129	0.229	0.125	0.224	0.124	0.224	0.125	0.224	0.168	0.263	0.127	0.224	0.167	0.263
ETTm1	96	0.305	0.359	0.301	0.354	0.303	0.355	0.296	0.351	0.336	0.382	0.299	0.355	0.335	0.378
	48	0.287	0.344	0.276	0.333	0.278	0.336	0.266	0.328	0.500	0.472	0.372	0.334	0.507	0.469
	24	0.246	0.312	0.223	0.293	0.218	0.293	0.196	0.279	0.473	0.429	0.225	0.305	0.487	0.434
	12	0.218	0.287	0.156	0.241	0.151	0.240	0.128	0.222	0.320	0.335	0.144	0.237	0.318	0.322
ETTm2	96	0.177	0.262	0.174	0.261	0.167	0.255	0.162	0.250	0.178	0.260	0.172	0.258	0.176	0.258
	48	0.139	0.238	0.137	0.236	0.145	0.248	0.143	0.250	0.167	0.264	0.148	0.249	0.157	0.253
	24	0.121	0.219	0.117	0.217	0.110	0.211	0.101	0.199	0.132	0.227	0.110	0.209	0.126	0.223
	12	0.086	0.175	0.083	0.174	0.083	0.174	0.078	0.169	0.089	0.178	0.082	0.172	0.088	0.178
PEMS03	96	0.171	0.280	0.153	0.263	0.149	0.258	0.143	0.252	0.360	0.416	0.147	0.257	0.223	0.329
	48	0.122	0.234	0.106	0.217	0.105	0.215	0.102	0.210	0.299	0.380	0.109	0.216	0.202	0.317
	24	0.089	0.201	0.079	0.187	0.081	0.188	0.075	0.181	0.097	0.209	0.082	0.189	0.129	0.244
	12	0.067	0.173	0.063	0.167	0.065	0.169	0.062	0.165	0.078	0.185	0.067	0.177	0.089	0.199

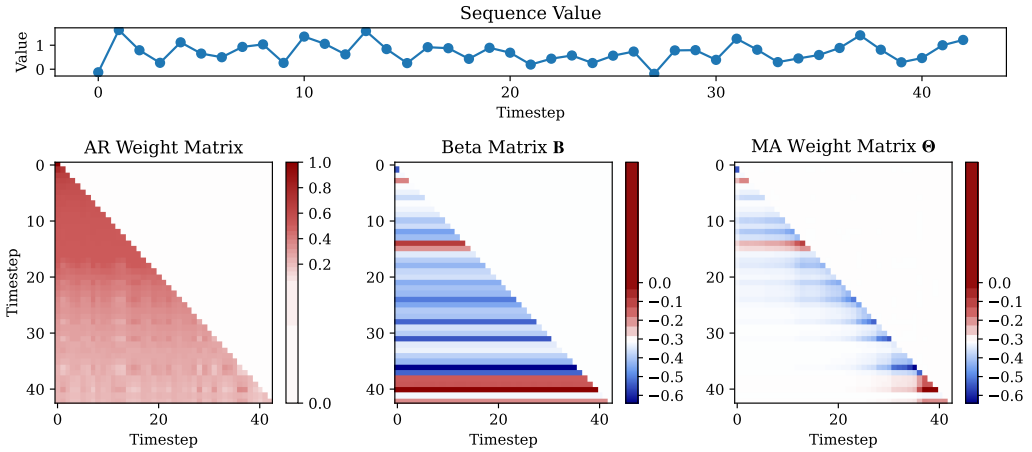

(a) Dataset: Weather, Channel: 1st, Layer: 1st

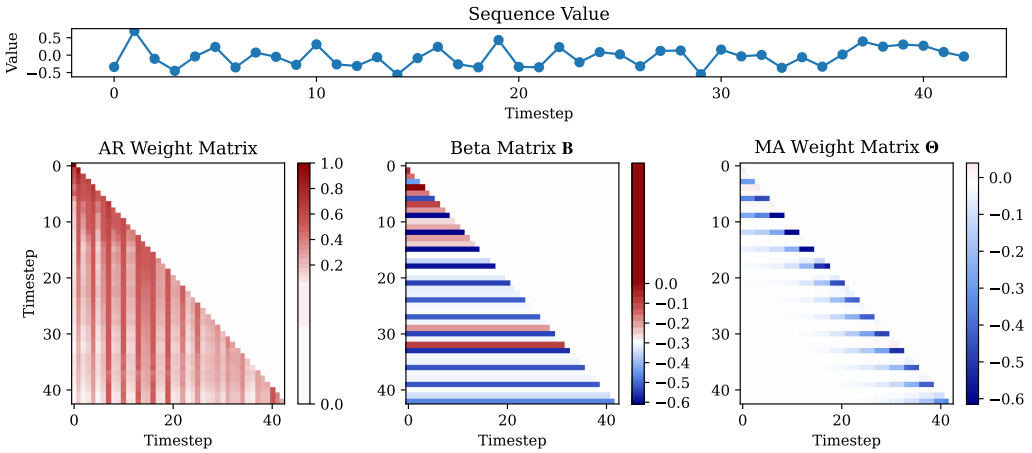

(b) Dataset: Weather, Channel: 1st, Layer: 2nd

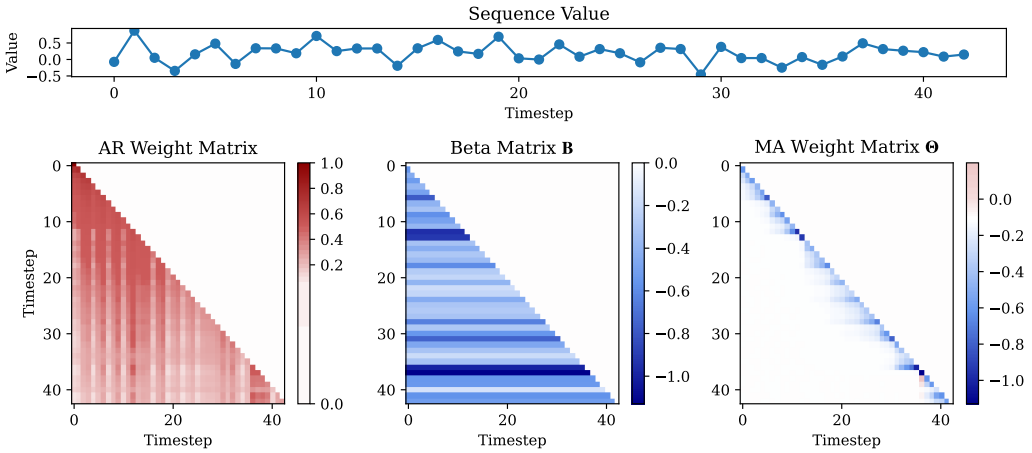

(c) Dataset: Weather, Channel: 1st, Layer: 3rd

Figure 9: Visualization of the ARMA attention weights of the first input channel for the first test set data point in the Weather dataset ($L_I = 4096$, $L_P = 96$).

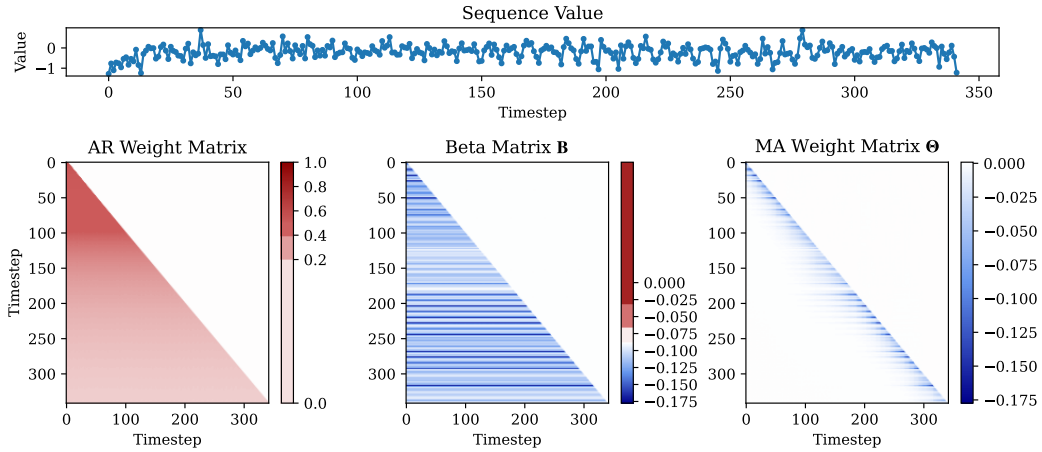

(a) Dataset: ETTm1, Channel: 1st, Layer: 1st

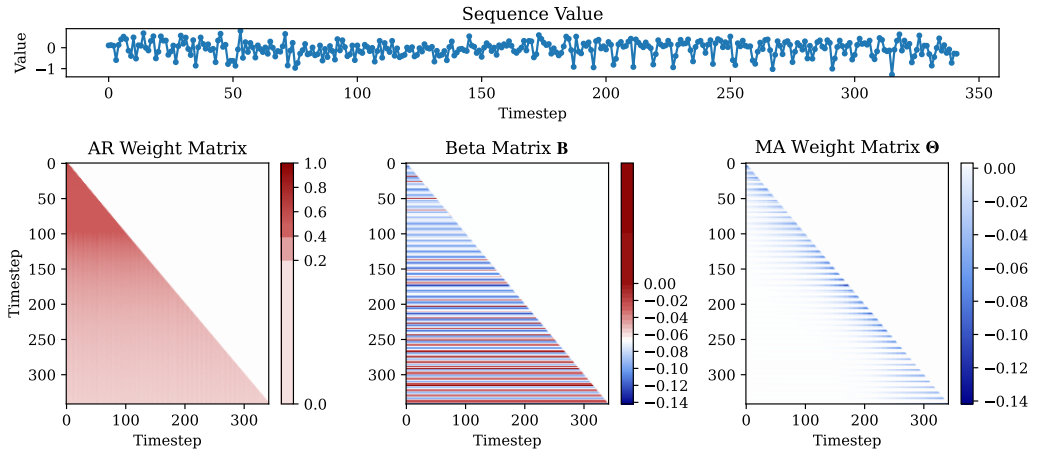

(b) Dataset: ETTm1, Channel: 1st, Layer: 2nd

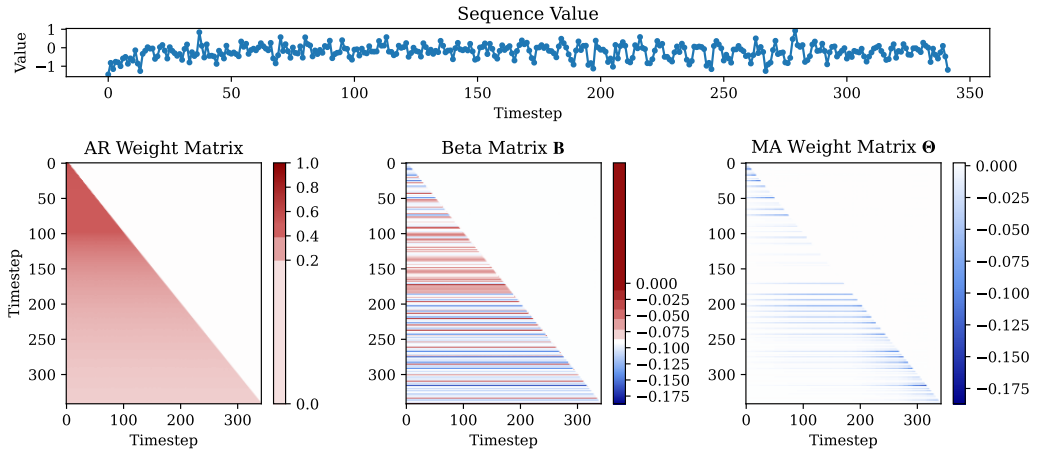

(c) Dataset: ETTm1, Channel: 1st, Layer: 3rd

Figure 10: Visualization of the ARMA attention weights of the first input channel for the first test set data point in the ETTm1 dataset ($L_I = 4096$, $L_P = 12$).

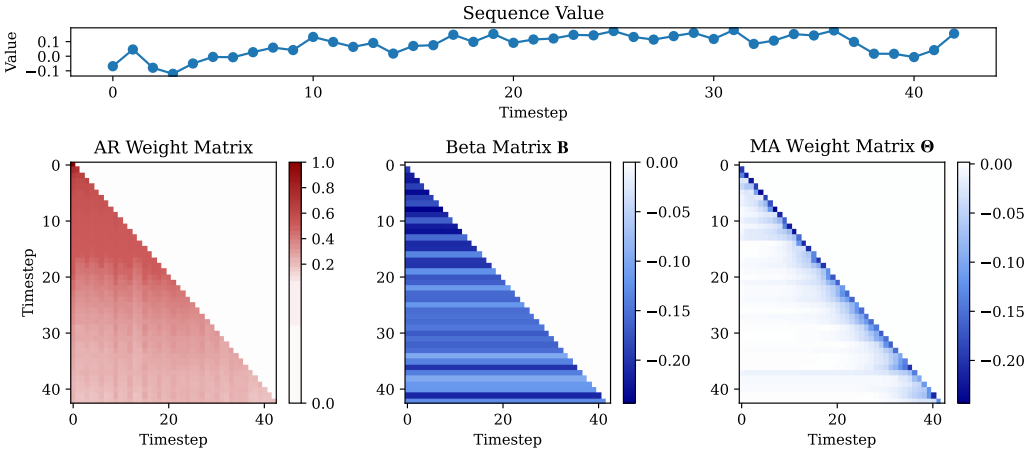

(a) Dataset: Weather, Channel: All (Averaged), Layer: 1st

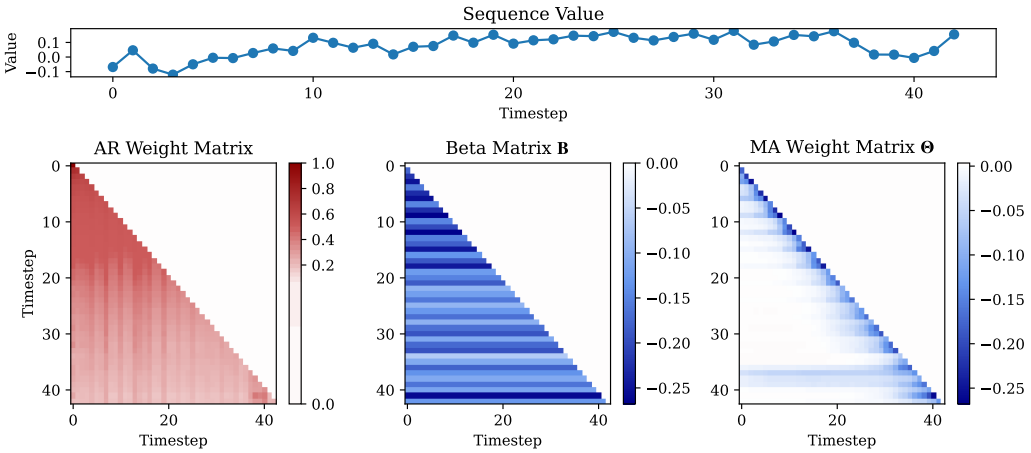

(b) Dataset: Weather, Channel: All (Averaged), Layer: 2nd

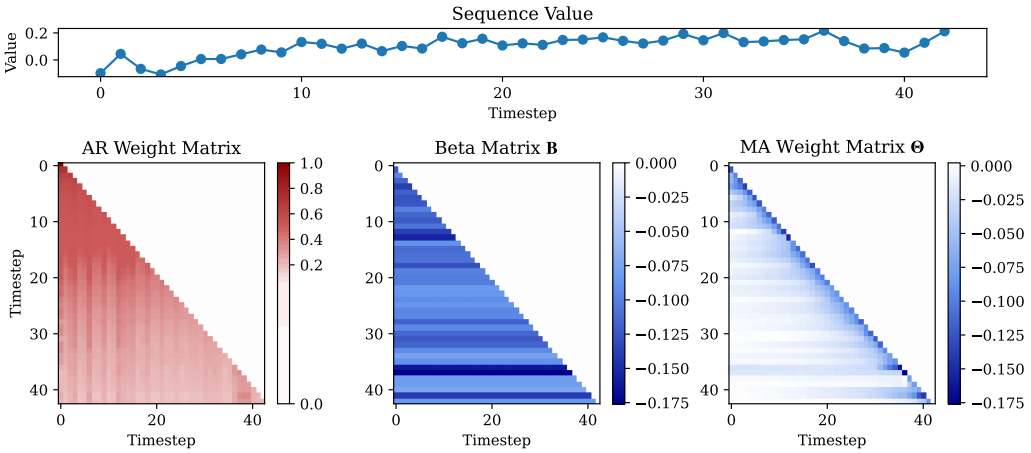

(c) Dataset: Weather, Channel: All (Averaged), Layer: 3rd

Figure 11: Visualization of the ARMA attention weights for the first test set data point in the Weather dataset ($L_I = 4096$, $L_P = 96$).

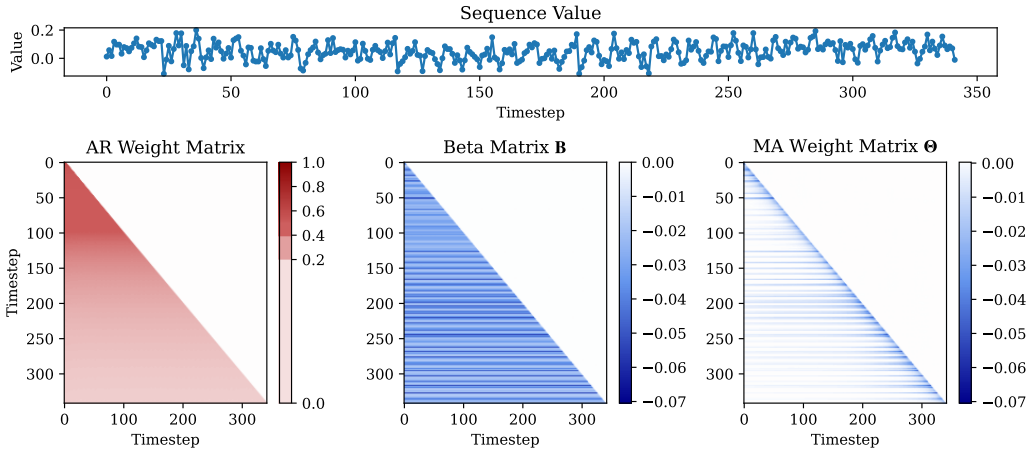

(a) Dataset: ETTm1, Channel: All (Averaged), Layer: 1st

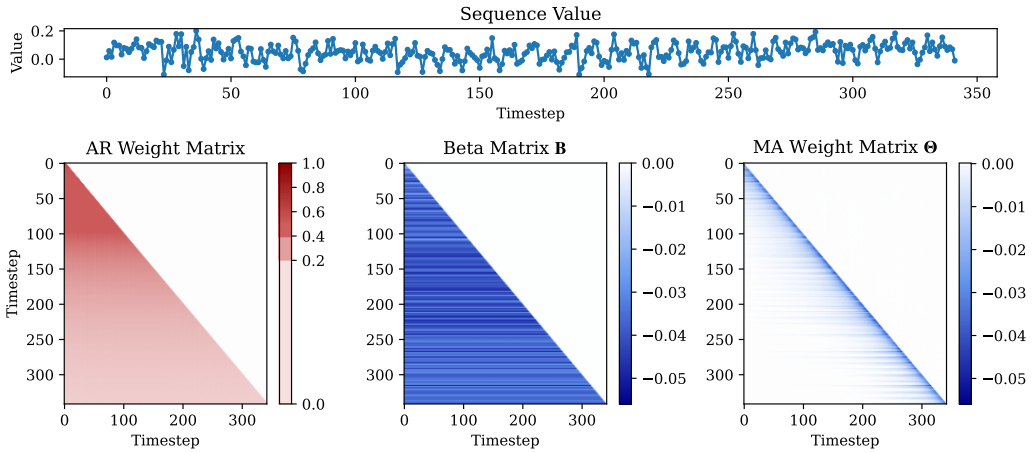

(b) Dataset: ETTm1, Channel: All (Averaged), Layer: 2nd

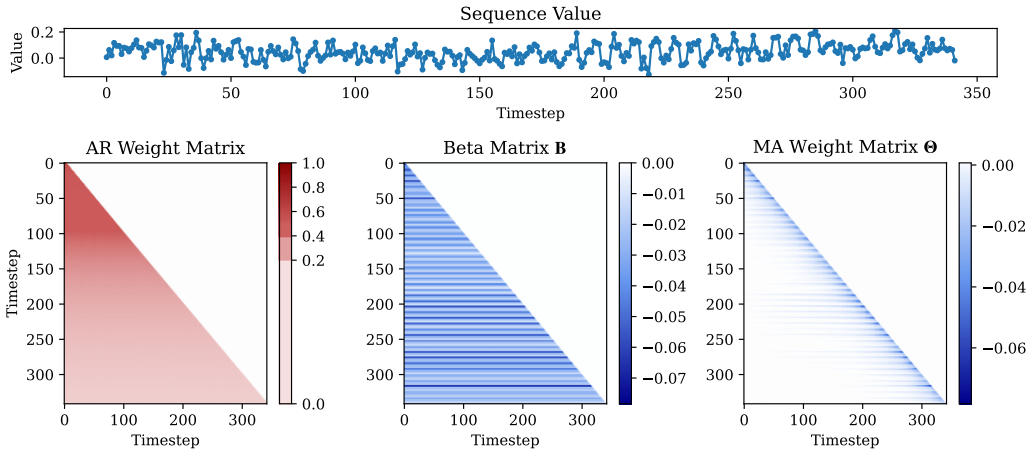

(c) Dataset: ETTm1, Channel: All (Averaged), Layer: 3rd

Figure 12: Visualization of the ARMA attention weights for the first test set data point in the ETTm1 dataset ($L_I = 4096$, $L_P = 12$).